THE GEOLOGICAL SOCIETY OF AMERICA®

Eocene Basalt of Summit Creek: Slab breakoff magmatism in the central Washington Cascades, USA

Lisa B. Kant[1,*], Jeffrey H. Tepper[1], Michael P. Eddy[2], and Bruce K. Nelson[3]

[1]GEOLOGY DEPARTMENT, UNIVERSITY OF PUGET SOUND, 1500 NORTH WARNER AVENUE, TACOMA, WASHINGTON 98416-1048, USA
[2]DEPARTMENT OF GEOSCIENCES, PRINCETON UNIVERSITY, GUYOT HALL, PRINCETON, NEW JERSEY 08544, USA
[3]DEPARTMENT OF EARTH AND SPACE SCIENCES, UNIVERSITY OF WASHINGTON, BOX 351310, 4000 15TH AVENUE NE, SEATTLE, WASHINGTON 98195-1310, USA

ABSTRACT

The early Eocene (52–44 Ma) was a time of tectonic reorganization and widespread magmatism in Washington, Oregon, and British Columbia (west coast of the United States and Canada) that culminated with establishment of the Cascade arc. Details of this tectonic transition remain enigmatic, and diverse scenarios involving ridge-trench interaction, slab breakoff, and/or plume magmatism have been proposed. This study focuses on the ca. 48 Ma Basalt of Summit Creek, a ~1500-m-thick sequence of subaerial lavas that erupted during the interval of time between accretion of the Siletzia terrane to the west and inception of the Cascade arc. The sequence dominantly consists of moderately evolved tholeiitic basalts (9.3–3.1 wt% MgO; Mg# = 0.66–0.29) and scarce rhyolites that erupted in the forearc but are chemically and isotopically similar to oceanic basalts of the Crescent Formation, found ~100 km to the west as part of the Siletzia terrane. Basalt of Summit Creek lavas lack subduction signatures (e.g., high field strength element depletions) and require a mechanism whereby asthenospheric melts were able to reach the surface having undergone little or no chemical interaction with fluids derived from the subducting slab or metasomatized mantle. We suggest that the accretion of Siletzia led to breakoff of the Farallon slab, and that Basalt of Summit Creek lavas formed by decompression melting of mantle that upwelled through the rupture. Slab breakoff typically produces a short-lived linear magmatic belt; the Basalt of Summit Creek appears to be part of such a belt, previously unrecognized, that parallels the Siletzia boundary and formed between 50 and 48 Ma.

LITHOSPHERE; v. 10; no. 6; p. 792–805; GSA Data Repository Item 2018359 | Published online 17 October 2018 https://doi.org/10.1130/L731.1

INTRODUCTION

Throughout Washington, Oregon, and British Columbia (west coast of the United States and Canada), the early to middle Eocene was a time of unusually widespread magmatism, extension, and tectonic reorganization. Within a span of less than 10 m.y., between ca. 52 and 44 Ma, major tectonic events in this region included accretion of the oceanic Siletzia terrane in western Washington, Oregon, and British Columbia (Wells et al., 2014), voluminous and compositionally diverse magmatism in the Challis-Kamloops belt (Fig. 1), which extends from central Washington northward into Canada and as far inland as Montana (Ewing, 1980; Dostal et al., 1998; Bordet et al., 2014), broad regional uplift (Dumitru et al., 2013), extension manifested by core complex formation (Kruckenberg et al., 2008; Gordon et al., 2009), rapid basin subsidence (Evans and Ristow, 1994; Eddy et al., 2016), dike swarm emplacement (Tabor et al., 1984; Miller et al., 2016), and establishment of the Cascade arc (Vance et al., 1987; Christiansen and Yeats, 1992; Sherrod and Smith, 2000).

Geologic events occurring during this time have been the subject of intensive research within the region. However, our understanding of the broader tectonic environment remains incomplete. It is well established that the west coast of North America has been a convergent margin since at least the Cretaceous (Dickinson and Snyder, 1978; Ewing, 1980), but within this framework, several models have been proposed to account for the Eocene structural and magmatic evolution of the region. Ewing (1980) attributed the width of the Challis-Kamloops belt to changes in the dip of the subducting Farallon slab. Noting the crustal character of Eocene volcanic rocks in eastern Washington and the contemporaneous extension, Morris et al. (2000) ascribed this activity to collapse of thickened crust, with no explicit role for mantle processes. More recently, based largely on plate-motion reconstructions and/or geochemistry, several authors have proposed that Challis-Kamloops belt magmatism developed during the passage of one or more slab windows beneath the region (Thorkelson and Taylor, 1989; Breitsprecher et al., 2003; Haeussler et al., 2003; Madsen et al., 2006). Alternatively, seismic anomalies in the mantle beneath the northwestern United States have been interpreted as detached fragments of the Farallon slab (Sigloch et al., 2008; Schmandt and Humphreys, 2011), suggesting that slab breakoff followed by rollback could have been the causal mechanisms for magmatism and uplift.

To better understand the tectonic processes that occurred during the Eocene, we studied the Basalt of Summit Creek (BSC), a sequence of basalts and minor rhyolite exposed within the boundaries of the younger Cascade arc in Washington state (Fig. 1). These lavas erupted in the critical time window during or slightly after the accretion of Siletzia but before the inception of the Cascade arc. In addition, the location of the BSC, east of the accreted oceanic rocks but west of the Challis belt, affords a rare opportunity to connect events occurring in the continental margin

Lisa Kant http://orcid.org/0000-0001-8822-8752
*Present address: Department of Geology and Geophysics, University of Wyoming, 1000 East University Avenue, Laramie, Wyoming 82071, USA.

© 2018 The Authors. Gold Open Access: This paper is published under the terms of the CC-BY-NC license.

Downloaded from http://pubs.geoscienceworld.org/gsa/lithosphere/article-pdf/10/6/792/4556618/792.pdf
by guest

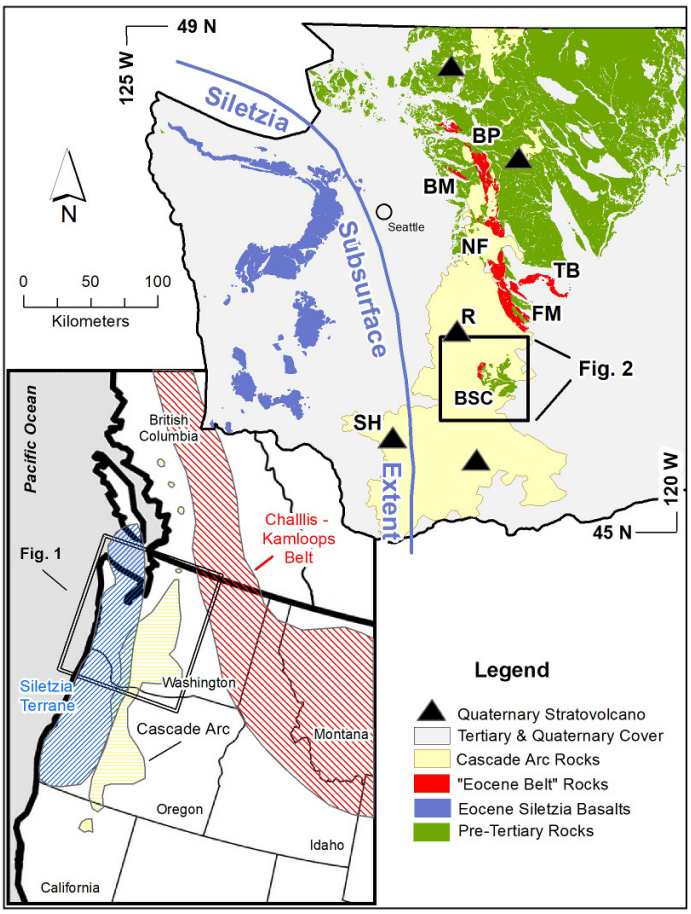

Figure 1. Simplified geologic map of western Washington. The inset map shows the western United States and Canada with the locations of Siletzia, the Cascade arc, and the Challis-Kamloops belt. The main figure shows the distribution of early "Eocene belt" rock units relative to Siletzia basalts and Cascade arc. The "Eocene belt" roughly parallels the inferred Siletzia margin in the subsurface (Trehu et al., 1994) and includes the Basalt of Summit Creek (BSC), the Basalt of Frost Mountain (FM), the Teanaway Basalt (TB), the Naches Formation (NF), the Mount Pilchuck Stock and Bald Mountain Batholith (BM), and the Barlow Pass volcanics (BP). Cascade stratovolcanos are marked with black triangles, which include Mount Rainier (R) and Mount St. Helens (SH).

or forearc region with those occurring farther inboard. In this paper, we combine major-element, trace-element, and Sr-Nd-Pb isotopic data with high-precision U-Pb geochronology to constrain the origin and tectonic setting of the BSC. These results provide insights into the history of the Farallon slab during and immediately after the accretion of Siletzia at the latitude of Washington, as well as the magmatic and tectonic manifestations of this event found farther inland.

Regional Geologic Context

The basement of the Cascadia forearc region consists of Paleocene and Eocene basalts that comprise the Siletzia terrane (Fig. 1). This terrane extends ~500 km from southern Oregon to southern Vancouver Island and consists of basalt with subordinate sedimentary and silicic volcanic rocks (Wells et al., 1984; Massey, 1986; Babcock et al., 1992; McCrory and Wilson, 2013; Wells et al., 2014). A notable feature of Siletzia is its great thickness. Mapping by Babcock et al. (1992) showed that >16 km of basalt flows are exposed in Washington, while seismic data indicate that the total thickness of the terrane thrust beneath Oregon is up to 20–30 km (Trehu et al., 1994). While an extreme stratigraphic thickness for the terrane has been previously suggested (Babcock et al., 1992), recent U-Pb dating has shown that the terrane is structurally thickened in Washington (Eddy et al., 2017). In Washington, rocks belonging to Siletzia are mapped as the Crescent Formation, which is dominantly composed of submarine and subaerial basalts that display a spectrum of mid-ocean-ridge basalt (MORB) and oceanic-island basalt (OIB) geochemical and isotopic affinities (Snavely et al., 1968; Muller, 1980; Babcock et al., 1992; Pyle et al., 2009). Recent geochronologic investigations suggest that Siletzia was emplaced between 56 and 48 Ma (Wells et al., 2014; Eddy et al., 2017). However, in Washington the age range of the basalts is limited to between 53 and 48 Ma (Eddy et al., 2017).

The large magma volumes calculated from the area-thickness data (~2 × 10^6 km^3; Trehu et al., 1994; Wells et al., 2014), relatively short duration of volcanism, Pb, Hf, Nd, and Sr isotopic evidence of a plume component, and plate reconstruction models that place the Yellowstone plume near the Oregon coast during the Paleogene have led to the conclusion that Siletzia originated as an oceanic plateau or chain of islands produced where a hotspot interacted with a spreading ridge, much like Iceland (Duncan, 1982; Wells et al., 1984; Massey, 1986; Murphy et al., 2003; Madsen et al., 2006; Pyle et al., 2009; McCrory and Wilson, 2013; Wells et al., 2014; Eddy et al., 2017; Phillips et al., 2017). This terrane accreted to North America during the Eocene, but the event was probably not synchronous along strike. Shortening within forearc sedimentary sequences in Washington indicates that the northern part of the terrane accreted between 51.3 and 49.9 Ma (Eddy et al., 2016); a 48.7 Ma sill in southwest Washington may record extensional stresses associated with establishment of the new subduction zone after accretion was complete (Moothart, 1993; Wells et al., 2014). The short span of time between eruption of Siletzia and its accretion to North America is consistent with the terrane having formed close to the continental margin. Postaccretion (ca. 42–35 Ma) mafic volcanism along the continental margin in Washington and Oregon has been attributed to subduction of a plume-influenced spreading ridge (Chan et al., 2012) or interaction between a plume and the continental margin (Parker et al., 2010; Wells et al., 2014).

The docking of Siletzia triggered a major reorganization of the North American margin at the latitude of Washington, Oregon, and British Columbia: The existing subduction zone was abandoned, and a new one was established farther to the west, outboard of the newly accreted terrane (Sigloch et al., 2008; Schmandt and Humphreys, 2011). Prior to this event, from ca. 65 to 50 Ma, there is only sparse evidence of magmatism in western Washington (Miller et al., 2016), although widespread Challis-Kamloops belt activity was under way to the east of the modern Cascades (Ewing, 1980; Thorkelson and Taylor, 1989; Dostal et al., 1998; Breitsprecher et al., 2003; Haeussler et al., 2003; Madsen et al., 2006; Bordet et al., 2014).

The establishment of the Cascade arc has traditionally been dated to ca. 37–36 Ma, although isolated exposures of calc-alkaline volcanic rocks suggest activity may have begun as early as 44 Ma (Christiansen and Yeats, 1992; Sherrod and Smith, 2000; MacDonald et al., 2013; Dragovich et al., 2016). In the central Washington Cascades, exposures of early Eocene igneous rocks are scarce, but among those with arc geochemical traits, there is an age gap between a volumetrically minor 53.7 Ma silicic tuff (this study) and ca. 42 Ma (Vance et al., 1987), a hiatus that coincides with Siletzia accretion. The BSC lavas were emplaced during this interval, along with six other rock units in western Washington that together define an arcuate belt, ~160 km long, that parallels the eastern boundary of Siletzia in the subsurface as inferred from seismic data (Fig. 1; Trehu

Downloaded from http://pubs.geoscienceworld.org/gsa/lithosphere/article-pdf/10/6/792/4556618/792.pdf
by guest

et al., 1994). Rocks in this belt cluster between 50 and 48 Ma in age and are notable for their petrologic diversity (Dragovich et al., 2016; Eddy et al., 2016). All of the volcanic units are bimodal, and many of the mafic rocks, including those in the BSC, have oceanic rather than arc chemical affinities (Tabor et al., 2000; Tanner and Tepper, 2016). Conversely, most of the felsic rocks in this belt, including tuffs and the S-type granites of the Mount Pilchuck stock and Bald Mountain pluton, have isotopic and petrologic traits indicative of crustal melting (Tabor et al., 2002; Dragovich et al., 2016).

Field Relations and Previous Geochronology

The BSC consists of an ~1500-m-thick section of subaerial basalt flows, interbedded with minor sandstone, shale, and tuff, that unconformably overlie highly deformed turbidites of the Rimrock Lake Inlier (Fig. 2), a dome-like uplift of Mesozoic basement rocks (Walsh et al., 1987; Miller, 1989). At least five scattered exposures of early to middle Eocene volcanic and sedimentary rocks exist along the margins of this uplift, but the section at Summit Creek is the oldest, thickest, and most complete (Vance et al., 1987; Walsh et al., 1987). The BSC is overlain by the late Eocene–Oligocene Ohanapecosh Formation, a voluminous package of subaerial and subaqueous tuffs and andesitic flows that range in age from 36 to 28 Ma and are interpreted as an early expression of the Tertiary Cascade arc (Vance et al., 1987). In the Summit Creek area, Ohanapecosh beds and BSC flows have the same steep (>60°) westward dips, suggesting they are concordant and underwent folding together, likely between 27 and 25 Ma (Vance et al., 1987), and implying that the BSC was approximately flat-lying prior to that time.

Summit Creek lava flows typically strike NNW to NNE and dip >60° to the west. These orientations appear consistent throughout the outcrop area; there is no indication of major internal deformation within the unit. Excellent exposures occur along U.S. Highway 12, which cuts through the section roughly perpendicular to strike (Fig. 2). Here, the flows are generally not more than a few meters thick, aphanitic to sparsely porphyritic, and massive or sparsely vesicular. Off the highway, outcrop is discontinuous, and indications of flow thickness or orientation, such as flow tops or vesicle horizons, are rarely discernible. Surface oxidation, calcite veins, vesicle fillings, and other signs of alteration and weathering are common, as are younger andesitic dikes and sills related to the Tertiary Cascade arc. Discontinuous patches of sedimentary rock and tuff occur at the contact between the BSC and the underlying basement rock. Along Highway 12, these include ~8 m of black shale overlain by ~12 m of fluvial sandstone and pebble conglomerate–bearing clasts derived from the underlying Mesozoic units (Vance et al., 1987).

Vance et al. (1987) determined an age range of 55–45 Ma for the BSC, bracketed by a 55 ± 3 Ma U-Pb zircon age on an underlying lapilli tuff (which has arc chemical affinities and is part of an earlier magmatic episode that predates the BSC) and two zircon fission-track ages of 46.1

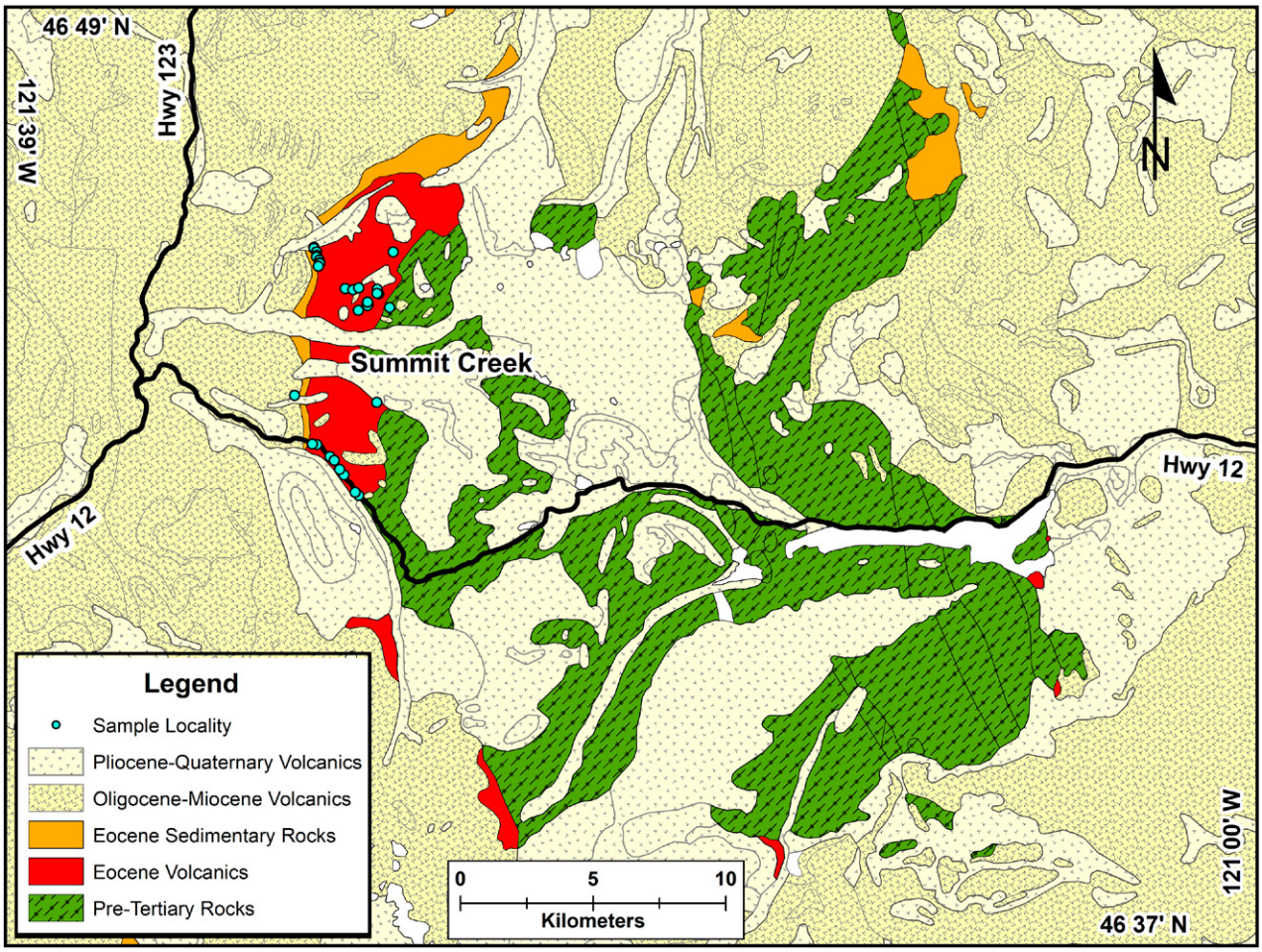

Figure 2. Simplified geologic map of the Summit Creek area after Walsh et al. (1987).

Downloaded from http://pubs.geoscienceworld.org/gsa/lithosphere/article-pdf/10/6/792/4556618/792.pdf
by guest

± 2.7 Ma and 44.0 ± 3.9 Ma from tuffs inferred to be on strike with the upper part of the basalt section. Two other small exposures of Eocene volcanic units that overlie the Rimrock Lake Inlier south of the BSC (Fig. 2) were also dated by Vance et al. (1987) and yielded fission-track ages of 41.8–42.4 ± 3.8 Ma. These units are roughly age equivalent to the late Eocene Northcraft volcanics that occur to the west (Phillips et al., 1988) and probably represent early stages of Cascade arc magmatism. In the field, these units clearly differ from the BSC in that they contain significant proportions of intermediate and felsic rocks.

FIELD AND ANALYTICAL METHODS

Sample sites (available in the BSC sample locations supplement in the GSA Data Repository Item[1]) encompass the BSC outcrop area and include two transects roughly perpendicular to the strike of the section: one along US Highway 12 east of the junction with WA Highway 123 (Fig. 2), and a second roughly five km farther north in the Gifford-Pinchot National Forest. Samples were chosen for analysis based on stratigraphic position and extent of post-eruptive alteration and weathering. Mineralogical and textural properties of BSC lavas were determined by petrographic examination of 11 representative samples. Mineral compositions (feldspar, pyroxene, Fe-Ti oxides) were measured on a JEOL 733 electron microprobe at the University of Washington.

Zircons were separated from two silicic volcanic rocks and dated using chemical abrasion-isotope dilution-thermal ionization mass spectrometry (CA-ID-TIMS) following methods slightly modified from Mattinson (2005) and described in Appendix A of Eddy et al. (2016). All measurements were made on either the VG Sector 54 or Isotopix X62 thermal ionization mass spectrometer (TIMS) at the Massachusetts Institute of Technology using the EARTHTIME ^{205}Pb-^{233}U-^{235}U isotopic tracer (Condon et al., 2015; McLean et al., 2015) and are presented in Table 1. We corrected for Pb fractionation using α = 0.25 ± 0.04 % (2σ, Sector 54) or 0.18 ± 0.04 % (2σ, X62) based on repeat measurements of the NBS-981 Pb isotopic standard and U fractionation using the known ratio of ^{233}U/^{235}U in the EARTHTIME ^{205}Pb-^{233}U-^{235}U (ET535) isotopic tracer and assuming a zircon ^{238}U/^{235}U of 135.818 ± 0.045 (2σ: Hiess et al., 2012). We assume that all ^{204}Pb arises from laboratory contamination and corrected for this contamination using an isotopic composition of common lead of ^{206}Pb/^{204}Pb = 18.145833 ± 0.475155 (1σ abs.) ^{207}Pb/^{204}Pb = 15.303903 ± 0.295535 (1σ abs.) and ^{208}Pb/^{204}Pb = 37.107788 ± 0.875051 (1σ abs.) based on 149 procedural blanks measured in the MIT isotope geochemistry laboratory between 2009 and 2015. A correction for initial secular disequilibrium in the ^{238}U-^{206}Pb decay chain due to exclusion of Th during zircon crystallization was done using a [Th/U]magma = 2.8 ± 1 (2σ, abs.), which encompasses the range of [Th/U] seen in most felsic tuffs (Machlus et al., 2015). All data reduction was done using the UPb_Redux software package (Bowring et al., 2011) using the methods outlined in McLean et al. (2011) and the decay constants presented in Jaffey et al. (1971). Uncertainties are reported in the format ± X/Y/Z, where X is the analytical uncertainty, Y incorporates uncertainty related to the calibration of the ET535 tracer, and Z includes the uncertainty in the Jaffey et al. (1971) decay constants. We use the expected 2σ variability in the mean square of weighted deviates (MSWD, Wendt and Carl, 1991) to assess whether a group of zircon dates forms a single population within analytical uncertainty, and report weighted mean eruption/deposition ages for the two samples below.

TABLE 1. CHEMICAL ABRASION–ISOTOPE DILUTION–THERMAL IONIZATION MASS SPECTROMETRY (CA-ID-TIMS) U-Pb ZIRCON GEOCHRONOLOGY RESULTS

	Dates								Composition			Isotopic ratios							
Frac.	^{206}Pb/^{238}U*	2σ abs.	^{207}Pb/^{235}U†	2σ abs.	^{207}Pb/^{206}Pb†	2σ abs.	% disc.§	Corr. coef.	Th/U#	Pb_c (pg)**	Pb*/Pb_c††	^{206}Pb/^{204}Pb§§	^{208}Pb/^{206}Pb##	^{206}Pb/^{238}U*,##	2σ %	^{207}Pb/^{235}U##	2σ %	^{207}Pb/^{206}Pb*,##	2σ %
SC12-20																			
z2	53.78	0.11	53.8	1.2	57	55	6.15	0.471	0.49	0.17	10.2	627	0.158	0.008364	0.2	0.0544	2.4	0.0472	2.3
z3	53.718	0.04	53.76	0.39	60	17	10.26	0.208	0.44	0.29	33.8	2067	0.139	0.0083535	0.074	0.05437	0.74	0.04723	0.73
z4	53.8	0.13	54.5	1.6	89	71	39.76	0.335	0.45	0.29	6.9	433	0.145	0.008367	0.25	0.0551	3.1	0.0478	3
z5	53.71	0.18	52.9	2.3	22	100	–148.46	0.339	0.42	0.91	4.8	309	0.136	0.008353	0.34	0.0535	4.4	0.0465	4.3
z6	53.99	0.27	54.3	3.2	73	140	26.17	0.392	0.44	0.27	3.6	237	0.141	0.008396	0.5	0.055	6	0.0475	5.8
z7	53.91	0.17	53.1	1.5	19	68	–186.75	0.486	0.45	0.18	9.6	600	0.145	0.008384	0.31	0.0536	3	0.0464	2.8
z8	53.76	0.1	53.5	1.3	44	57	–21.86	0.359	0.42	0.38	9.1	573	0.135	0.00836	0.19	0.0541	2.4	0.0469	2.4
NC-MPE-390																			
z4	48.15	0.12	47.3	1.6	11	81	–346.82	0.351	0.55	0.37	6.6	404	0.177	0.007484	0.26	0.0477	3.5	0.0463	3.4
z7	48.84	0.088	49.7	1.1	95	50	48.73	0.463	0.52	0.28	12	731	0.165	0.007591	0.18	0.0502	2.2	0.0479	2.1
z8	48.49	0.25	49.1	3.3	84	160	42.07	0.34	0.53	0.81	3.1	203	0.17	0.007536	0.53	0.0495	6.8	0.0477	6.6
z9	48.85	0.11	46.9	1.4	–47	71	204.36	0.39	0.53	0.29	7.9	483	0.171	0.007594	0.23	0.0473	3	0.0452	2.9
z10	48.517	0.094	47.8	1.2	16	62	–197.35	0.282	0.56	0.28	8.8	531	0.179	0.007541	0.2	0.0482	2.6	0.0464	2.6
z12	48.032	0.062	47.48	0.71	24	36	–99.15	0.348	0.47	0.16	16.6	1018	0.149	0.0074646	0.13	0.04787	1.5	0.04653	1.5
z13	48.102	0.08	47.22	0.78	7	39	–554.78	0.424	0.38	0.17	15.5	973	0.121	0.007475	0.17	0.0476	1.7	0.04621	1.6
z14	48.122	0.071	47.73	0.79	33	39	–47.7	0.428	0.48	0.21	14.5	885	0.153	0.007479	0.15	0.04813	1.7	0.04669	1.6
z15	48.22	0.08	48.23	0.84	53	41	9.99	0.471	0.41	0.2	15.1	936	0.131	0.007494	0.17	0.04865	1.8	0.0471	1.7

*Corrected for initial Th/U disequilibrium using radiogenic ^{208}Pb and Th/U[Magma] = 2.8 ± 0.5.
†Isotopic dates calculated using the decay constants λ238 = 1.55125E–10 and λ235 = 9.8485E–10 (Jaffey et al., 1971).
§% discordance = 100 – (100 × [^{206}Pb/^{238}U date]/[^{207}Pb/^{206}Pb date]).
#Th contents calculated from radiogenic ^{208}Pb and the ^{207}Pb/^{206}Pb date of the sample, assuming concordance between U-Th and Pb systems.
**Total mass of common Pb.
††Ratio of radiogenic Pb (including ^{208}Pb) to common Pb.
§§Measured ratio corrected for fractionation and spike contribution only.
##Measured ratios corrected for fractionation, tracer, and blank.

[1]GSA Data Repository Item 2018359, Basalt of Summit Creek major- and trace-element data, sample locations, and regional data and sources, is available at http://www.geosociety.org/datarepository/2018 or on request from editing@geosociety.org.

Downloaded from http://pubs.geoscienceworld.org/gsa/lithosphere/article-pdf/10/6/792/4556618/792.pdf
by guest

TABLE 2. REPRESENTATIVE GEOCHEMICAL DATA FOR THE BASALT OF SUMMIT CREEK

Sample	SC10-16	SC10-028	SC10-193	SC11-03	SC12-14	SC13-04
Major oxide (wt%)*						
SiO_2	47.53	52.05	48.72	51.27	49.72	81.72
TiO_2	1.30	1.28	1.16	1.56	1.46	0.17
Al_2O_3	16.92	15.19	16.14	16.27	16.36	11.28
Fe_2O_3T†	11.24	11.51	10.78	11.43	11.52	1.47
MgO	8.70	8.27	9.16	5.60	6.46	0.06
MnO	0.22	0.20	0.17	0.20	0.17	<0.01
CaO	11.76	7.41	11.75	10.48	9.92	0.06
Na_2O	2.09	3.67	1.91	2.83	4.24	1.27
K_2O	0.12	0.28	0.08	0.14	0.01	3.95
P_2O_5	0.12	0.13	0.12	0.22	0.15	0.01
LOI§	7.82	3.76	3.19	2.20	4.37	1.69
ORIG TOTAL	102.20	100.20	101.09	101.48	99.27	100.20
Mg #	0.61	0.59	0.63	0.49	0.53	0.08
Trace elements (ppm)						
Sc	40		35			
Cr	360	30	480	70	170	<10
V	350	195	281	280	318	<5
Ba	64.2	32.0	40.1	82.3	64.5	984.0
Rb	3.3	14.9	0.4	1.2	1.2	137.0
Sr	162.0	160.5	165.0	197.5	167.5	16.1
Cs	0.14	2.16	0.30	0.36	0.22	1.36
U	0.15	0.62	0.18	0.34	0.43	2.61
Th	0.43	1.91	0.89	1.24	1.24	12.45
Hf	2.2	5.5	2.2	3.2	2.4	12
Zr	88	231	83	120	84	350
Nb	5.4	20.8	8.0	9.9	3.5	41.3
Ta	0.5	1.5	0.7	0.8	0.3	2.8
La	5.1	18.9	7.2	11.4	7.5	31.2
Ce	12.6	41.4	15.4	24.2	17.8	92.6
Pr	1.88	5.57	2.25	3.18	2.52	9.09
Nd	9.3	24.9	9.5	14.0	12.3	33.2
Sm	2.89	6.49	3.47	3.58	3.45	7.18
Eu	1.19	2.36	1.23	1.32	1.37	1.08
Gd	4.03	8.17	4.16	4.03	4.50	6.14
Tb	0.65	1.28	0.70	0.70	0.71	0.93
Dy	4.14	7.76	4.08	4.41	4.83	4.87
Ho	0.83	1.58	0.89	0.92	1.01	1.15
Er	2.63	4.92	2.78	2.45	2.96	3.20
Tm	0.40	0.72	0.49	0.37	0.44	0.60
Yb	2.36	4.22	2.75	2.32	2.71	4.57
Lu	0.34	0.64	0.43	0.37	0.43	0.73
W	37	22	41		1	
Y	23.9	43.9	20.9	23.6	26.3	

*Major oxides are normalized to 100% anhydrous.
†Total Fe expressed as Fe_2O_3.
§LOI—loss on ignition.

A total of 39 BSC samples were trimmed to remove weathered material and prepared for whole rock isotopic and major and trace element analyses, the results of these analyses are contained in Table 2. Samples for isotopic and trace element analysis were pulverized in an alumina shatterbox; all other samples were pulverized in tungsten carbide. Powdered samples were fused using $LiBO_4$, dissolved in HNO_3, and analyzed for their major element compositions using inductively coupled plasma-optical emission spectrometry (ICP-OES), either at the University of Puget Sound or at ALS minerals in Vancouver, British Columbia. Loss on Ignition (LOI) was determined gravimetrically after firing for one hour at 1000 °C. Trace element compositions of 28 samples were also measured by inductively coupled plasma-mass spectrometry (ICP-MS) at ALS Minerals.

Isotopic analyses (Sr-Nd-Pb) of seven samples that reflect the chemical and stratigraphic diversity of the BSC were performed at the University of Washington using a Nu Instruments multicollector (MC) ICP-MS. Strontium and Nd were separated according to the procedures outlined in Nelson (1995). Analyses followed Brach-Papa et al. (2009) for Sr and Gaffney et al. (2007) for Nd. Lead separation and MC-ICP-MS analytical procedures were described in Harkins et al. (2008). To assess the isotopic effects of alteration three samples were analyzed in duplicate, one aliquot of each leached with 6M HCl at 93°C for 30 minutes prior to dissolution. The results of these leaching experiments (Table 3) indicate that for Nd the differences between leached and unleached samples are comparable to analytical uncertainty (0.1-0.3 ε_{Nd}); while for Pb, although leaching effects are greater (up to 0.15% for $^{208}Pb/^{204}Pb$), the effect is not large enough to significantly alter our interpretations. The impact of leaching on measured $^{87}Sr/^{86}Sr$ ratios is up to 160 ppm and not always toward a less radiogenic composition, although initial ratios of leached samples tend to be lower (0.70315–0.70331) than those of the unleached samples (0.70320–0.70389). This suggests while Sr and Nd isotopic data generally covary as expected, a portion of the $^{87}Sr/^{86}Sr$ variation could be the result of low temperature alteration.

RESULTS

Petrography

Most BSC lavas are aphanitic to sparsely porphyritic, and some contain amygdules. Normally zoned plagioclase (An_{66}-An_{28}) is the dominant phenocryst, ranging up to 3 mm long and in some cases forming glomerocrysts. Clinopyroxene (Mg# 0.87–0.68) is common in the groundmass but

TABLE 3. Sr-Nd-Pb ISOTOPE DATA FOR THE BASALT OF SUMMIT CREEK

Sample	$^{87}Rb/^{86}Sr$	$^{87}Sr/^{86}Sr$*	$^{87}Sr/^{86}Sr(i)$*	±2σ†	$^{147}Sm/^{144}Nd$	$^{143}Nd/^{144}Nd$*	$^{143}Nd/^{144}Nd(i)$*	±2σ†	$\varepsilon_{Nd}(i)$§	±2σ†	$^{206}Pb/^{204}Pb$**	$^{207}Pb/^{204}Pb$**	$^{208}Pb/^{204}Pb$**
SC10-16	0.058912	0.703240	0.703200	20	0.366261	0.513014	0.512899	12	6.32	0.23	19.044	15.533	38.624
SC10-16L††	0.058912	0.703354	0.703314	14	0.366250	0.513030	0.512915	8	6.63	0.16	19.005	15.538	38.560
SC10-22	0.160676	0.703736	0.703626	18	0.283253	0.512967	0.512878	12	5.91	0.23	19.046	15.592	38.630
SC10-164	0.215315	0.703470	0.703323	14	0.262754	0.512971	0.512889	10	6.11	0.20	19.047	15.591	38.629
SC10-164L††	0.215311	0.703306	0.703159	16	0.262750	0.512980	0.512898	14	6.29	0.27	19.054	15.589	38.628
SC10-193	0.145277	0.703795	0.703790	16	0.203442	0.512999	0.512864	12	5.63	0.23	19.076	15.552	38.628
SC11-03	0.017572	0.703529	0.703517	16	0.301406	0.512984	0.512889	10	6.13	0.20	19.120	15.551	38.669
SC11-03L††											19.087	15.548	38.616
SC12-14	0.020720	0.703900	0.703885	26							19.060	15.593	38.714
SC12-18	0.011745	0.703511	0.703503	26	0.337246	0.512832	0.512899	12	6.32	0.23	19.102	15.542	38.656

*Initial values were calculated assuming an age of 48 Ma. Sr and Nd compositions were normalized to $^{86}Sr/^{88}Sr$ = 0.1194 and 146Nd/^{144}Nd = 0.7219.
†Errors shown are within-run statistics. The following is the external reproducibility at 2σ: Nd = ±30 ppm; Sr = ±30 ppm; Pb = ±125, 150, and 200 ppm for $^{206}Pb/^{204}Pb$, $^{207}Pb/^{204}Pb$, and $^{208}Pb/^{204}Pb$, respectively.
§εNd(i) is the deviation from chondritic $^{144}Nd/^{143}Nd$ at 48 Ma in units of parts per 104 (modern value of chondritic $^{144}Nd/^{143}Nd$ = 0.512638).
**Pb isotope compositions were normalized to NIST-981 accepted values of $^{206}Pb/^{204}Pb$ = 16.937, $^{207}Pb/^{204}Pb$ = 15.491, and $^{208}Pb/^{204}Pb$ = 36.721.
††Leached with 6 M HCl at 93 °C for 30 min to remove Sr and Pb from surface alteration and fractures.

Downloaded from http://pubs.geoscienceworld.org/gsa/lithosphere/article-pdf/10/6/792/4556618/792.pdf
by guest

rare as a phenocryst. Fe-Ti oxides are present mainly in the groundmass and constitute over 10% of the mode in some of the more differentiated rocks. The groundmass is typically microcrystalline, accompanied in some cases by interstitial patches of green secondary minerals that may represent altered glass. Minor alteration is pervasive and includes amygdule fillings, veins of calcite, oxidation of mafic silicates, and partial replacement of primary minerals by epidote, sericite, and other secondary phases.

U-Pb Zircon Geochronology

Sample SC12–20 was collected from an ash-flow tuff near the base of the section and gives a weighted mean age of 53.744 ± 0.032/0.043/0.072 Ma (n = 7, MSWD = 1.8), which we interpret as the age of eruption/deposition (Fig. 3A). This tuff has arc-like chemical affinities such as high field strength element (HFSE) depletions and large ion lithophile element (LILE) enrichment, indicating that it was part of an earlier magmatic episode that predates both the BSC and establishment of the Cascade arc. This tuff provides a maximum age for the onset of BSC magmatism. Vance et al. (1987) obtained a U-Pb age of 55 ± 3 Ma from this unit (sample JV310). Sample NC-MPE-390 was collected from a rhyolite near the top of the section. The dispersion seen in all nine zircon dates from this sample greatly exceeds that expected for a single population (MSWD = 50). However, the youngest four grains overlap within uncertainty and give a weighted mean $^{206}Pb/^{238}U$ date of 48.086 ± 0.086/0.055/0.075 Ma (n = 4, MSWD = 1.8), which we interpret as the age of eruption/deposition (Fig. 3B). For this unit, Vance et al. (1987) determined a fission-track age of 46.1 ± 2.7 Ma (sample JV232).

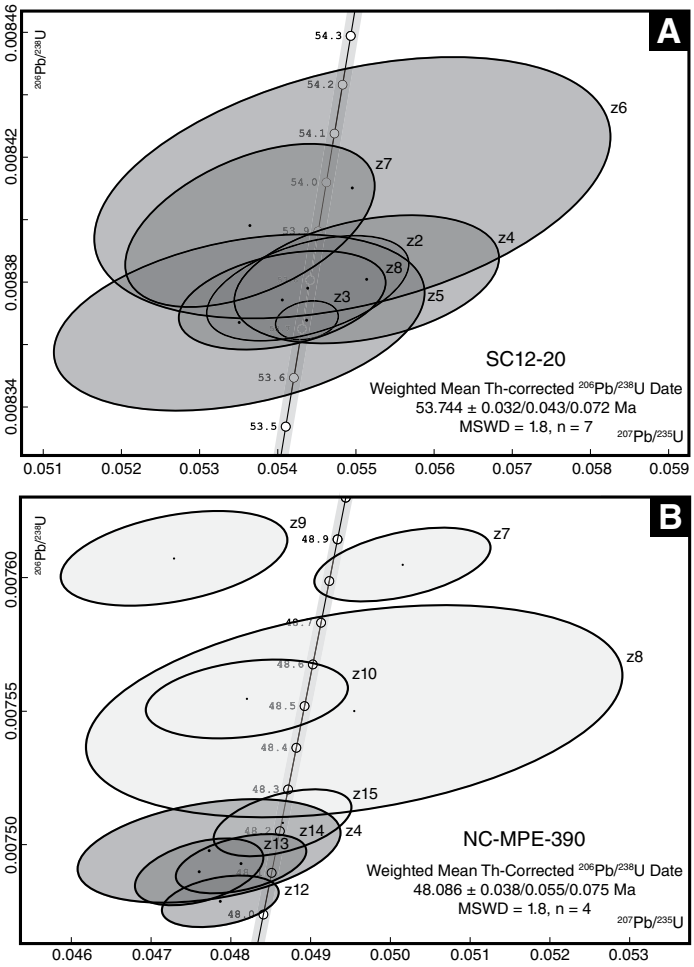

Figure 3. U-Pb concordia plots and weighted mean Th-corrected $^{206}Pb/^{238}U$ dates for (A) SC12–20 and (B) NC-MPE-390. Isotopic data are presented in Table 1. Analyses used in the weighted mean calculation are shown with darker shading. Those interpreted as antecrysts or xenocrysts are shown with lighter shading. All uncertainties are 2σ. MSWD—mean square of weighted deviates.

Geochemistry

The BSC is bimodal in composition, consisting dominantly of tholeiitic basalts and basaltic andesites with minor rhyolite (Table 2; Fig. 4; full BSC data set is available in the BSC major- and trace-element data supplemental material in the Data Repository Item). Considerable variation is present in Mg# (molar Mg/[Mg + Fe_{Total}]), which ranges from 0.66 to 0.29 (and to 0.08 if rhyolitic samples are included). In general, as Mg# decreases, CaO contents decline, TiO_2 and P_2O_5 contents rise to a maximum at Mg# ~0.4 and then decrease, Na_2O and K_2O contents increase steadily, and Al_2O_3 contents remain about the same (Fig. 5). However, major-element data show considerable scatter: CaO, for example, commonly varies by 3–4 wt% among samples with the same Mg# (Fig. 5). Trace-element concentrations show considerable variation and generally coherent trends, excluding a few samples for which there is isotopic evidence suggestive of source heterogeneity. With lower Mg#, Cr (550 to <10 ppm) and Ni (225 to <5 ppm) concentrations decrease markedly, while Zr concentrations increase steadily by a factor of 2–3, and V rises to a maximum at Mg# ~0.4 and then decreases (Fig. 5). With differentiation, other incompatible trace elements (e.g., rare earth elements [REEs], Ba, Zr, Nb, Th, U, Hf) increase by a factor of 3–4 (and up to 10 or more if rhyolitic samples are included). All BSC samples show moderate light (L) REE enrichment (La/Yb_N = 1.2–5.9; Fig. 6A) that varies modestly among samples with similar Mg# (~1–3 at Mg# = 60). Europium anomalies are small (Eu/Eu* = 1.2–0.9), except in the rhyolite samples (Eu/Eu* = 0.3–0.5). Primitive magmas (Mg# >62, Cr >300 ppm) are restricted to the lower part of the section; aside from this, no stratigraphic trends in composition are evident.

Roughly two thirds of the analyzed BSC samples have distinctly low K_2O and Rb contents, a characteristic clearly visible on a MORB-normalized spidergram (Fig. 6B). There is no correlation between alkali depletion and either Mg# or stratigraphic position, but in general the alkali-depleted samples also have lower concentrations of REEs, particularly LREEs, and HFSEs than their non-alkali-depleted counterparts (Fig. 6). Low-temperature alteration could have removed K and Rb but is unlikely to have affected REEs or HFSEs. In addition, there is no evidence that the alkali-depleted samples are more altered, as average LOI contents of the alkali-depleted samples (3.3 wt%) and non-alkali-depleted samples (3.4 wt%) are similar. These observations suggest that alkali depletion could be a primary feature of some BSC samples.

Initial ε_{Nd} values cluster between +6.6 and +5.6, whereas initial $^{87}Sr/^{86}Sr$ values are more variable, ranging from 0.70316 to 0.70389 (Table 3). These data overlap with the Sr-Nd isotopic compositions of Cascade arc rocks in general (Fig. 7A), but they have higher ε_{Nd} and lower $^{87}Sr/^{86}Sr$ values than samples from nearby Mount Rainier (Sisson et al., 2014). Compared to Crescent basalts (Tepper et al., 2008; Pyle et al., 2009; Sisson et al., 2014), BSC lavas display a nearly identical range of initial ε_{Nd} values but a more restricted range of initial $^{87}Sr/^{86}Sr$, with no ratios >0.704 (Figs. 7A and 7B). The BSC data define a slightly inclined linear array (Fig. 7A) that has no apparent correlation with indices of differentiation (e.g., Mg#, Cr content, or K_2O content) or stratigraphic position.

Downloaded from http://pubs.geoscienceworld.org/gsa/lithosphere/article-pdf/10/6/792/4556618/792.pdf
by guest

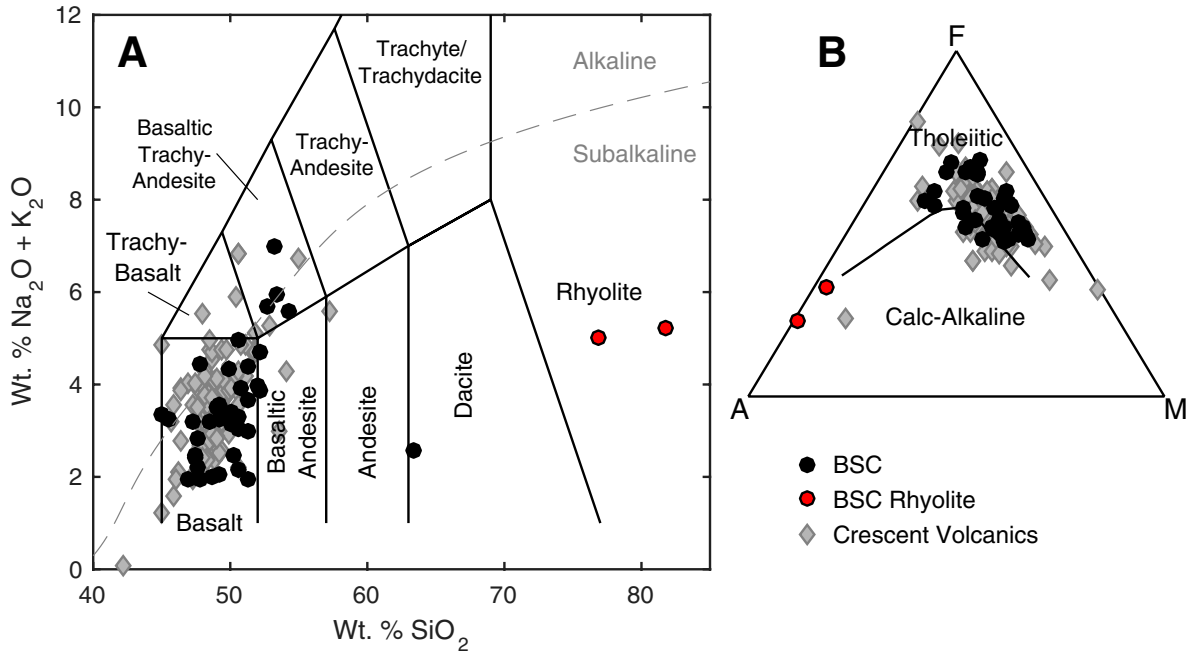

Figure 4. Geochemical classification diagrams for the Basalt of Summit Creek (BSC) with Crescent basalts for comparison. (A) Total alkalis vs. silica (Le Bas et al., 1986) showing that the BSC is subalkaline and dominantly basalt. (B) AFM diagram (Alkalis [$Na_2O + K_2O$] – FeO – MgO; Irvine and Baragar, 1971) showing that BSC lavas are primarily tholeiitic. Crescent Formation basalt data and sources are contained in the regional data supplemental material in the Data Repository (see text footnote 1).

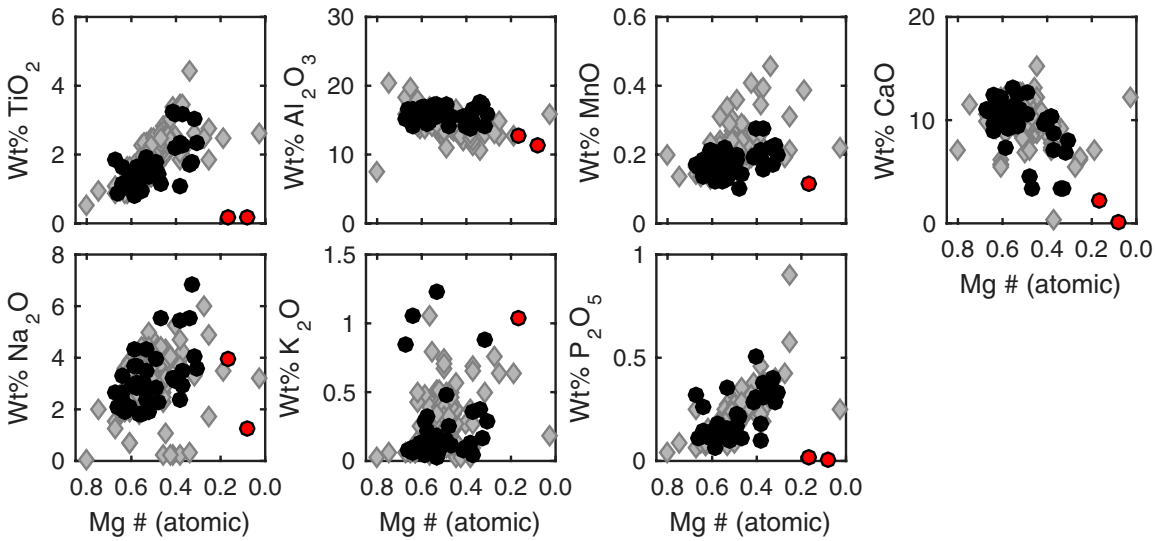

Figure 5. Variation diagrams for major elements against Mg# (molar Mg/[Mg + Fe_{Total}]), comparing the Basalt of Summit Creek and the Crescent Formation basalts. Symbols used are the same as those of Figure 4 (Crescent Formation basalt data and sources available in the regional data supplemental material in the Data Repository [see text footnote 1]).

Downloaded from http://pubs.geoscienceworld.org/gsa/lithosphere/article-pdf/10/6/792/4556618/792.pdf
by guest

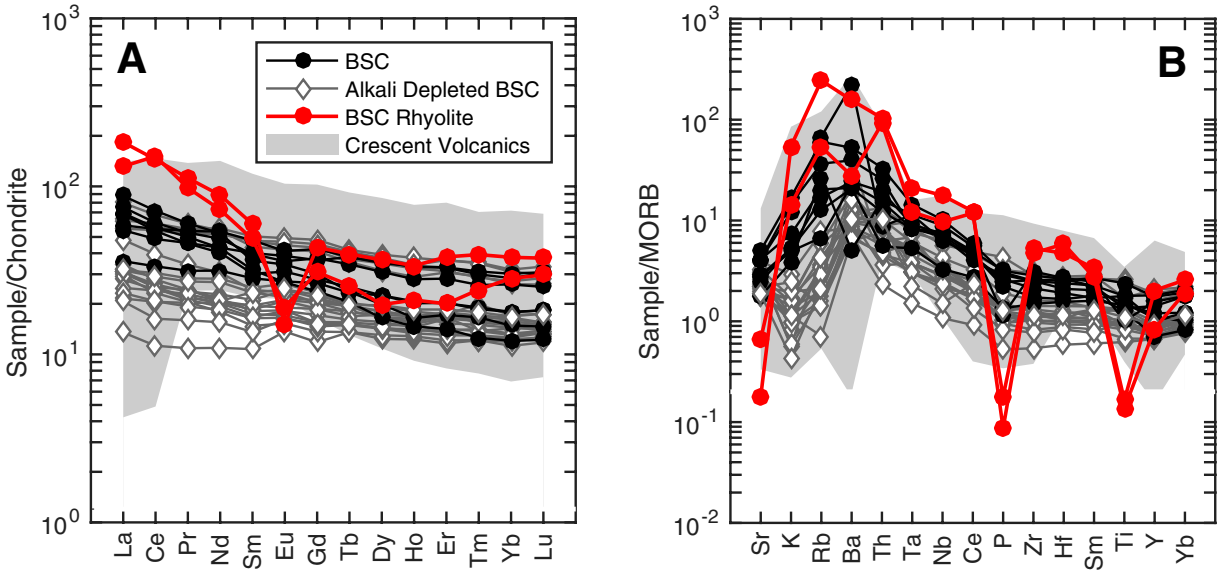

Figure 6. (A) Rare earth element (REE) data normalized to chondrite values of McDonough and Sun (1995). Most Basalt of Summit Creek (BSC) samples display modest light (L) REE enrichment, lack Eu anomalies, and are generally similar to the Crescent basalts (shaded gray field). (B) Spider diagram normalized to mid-ocean-ridge basalt (MORB) values of Sun and McDonough (1989). Most BSC samples have a convex profile typical of oceanic-island basalt, as is also seen among Crescent basalts (shaded gray field). Samples with Ta-Nb depletions characteristic of arc magmatism are also isotopically distinct from other BSC samples, with elevated $^{207}Pb/^{204}Pb$ values (Crescent Formation basalt data and sources available in the regional data supplemental material in the Data Repository [see text footnote 1]).

Measured Pb isotopic compositions of most BSC samples (Table 3; Figs. 7C and 7D) plot on or slightly below the Northern Hemisphere reference line (NHRL; Hart, 1984). These samples lie within the broad field of data for Crescent basalts (Pyle et al., 2009; Chan et al., 2012; Haileab et al., 2012; Sisson et al., 2014; Phillips et al., 2017). They are more radiogenic than modern Juan de Fuca MORB (White et al., 1987; Hegner and Tatsumoto, 1987) but generally less radiogenic than the late Eocene plume-related Grays River Volcanics (Chan et al., 2012). Pb concentrations of most BSC samples are below detection by the ICP-MS used (~2 ppm), which precludes calculation of initial Pb isotopic compositions. However, due to their low U and Th contents, even if Pb concentrations of these lavas were as low as typical MORB (0.5 ppm; Doe, 1994), the samples would still straddle the NHRL (Figs. 7C and 7D). Three BSC samples have higher $^{207}Pb/^{204}Pb$ values (15.589–15.593) than the others and cluster above the NHRL (Fig. 7C). These basalts (Mg# = 0.64–0.53) also have higher U and Th contents, and generally higher La/Yb and Ba/Nb, and one shows HFSE depletions on a spidergram.

DISCUSSION

Magma Evolution

Low Mg# values and low Cr concentrations indicate that most BSC lavas have undergone significant differentiation. To assess the role of fractional crystallization, we used MELTS (Ghiorso and Sack, 1995) to model the crystallization of potential parent magmas as well as constrain the pressure(s) at which differentiation occurred and the water content of the system. These calculations were performed assuming a parental magma similar in composition to the more primitive BSC samples (50.7 wt% SiO_2, 14.3 wt% Al_2O_3, 0.04 wt% K_2O, Mg# = 0.66). Pressure was varied from 0.1 to 10.0 kbar at constant water content of 0.2 wt% H_2O, and water contents were varied from 0.1 to 1.0 wt% H_2O at constant pressure (P) of 5 kbar.

The main effect of increasing either pressure or water content was to decrease the proportion of plagioclase relative to clinopyroxene in the fractionating assemblage. The impact of this shift on melt composition was most apparent in Al_2O_3 contents, and the best match between MELTS results and BSC data was obtained with H_2O <0.5 wt% and P = 1–5 kbar (Fig. 8), indicating that differentiation occurred mainly at mid- to upper-crustal depths. Using these conditions, the full range of BSC basalts and basaltic andesites (Mg# = 0.65–0.30) can be modeled by a maximum of 64%–77% fractionation of an assemblage dominated by clinopyroxene (52%–68%) and plagioclase (30%–43%) with lesser spinel, olivine, and orthopyroxene. While clinopyroxene phenocrysts are rare, MELTS results do not necessarily conflict with petrographic results. BSC samples are typically phenocryst poor, suggesting that early formed crystals, particularly ferromagnesian minerals, were separated from the magma prior to eruption. Further fractionation of a similar assemblage plus minor apatite and Fe-Ti oxides lead to highly evolved compositions (Mg# <0.20) that are similar to BSC rhyolites (Fig. 8). However, these rhyolites have concave-upward REE patterns (Dy/Yb_N <1; Fig. 6A) that point to involvement of amphibole (Davidson et al., 2007), a phase that cannot be modeled with the existing version of MELTS. In view of the wide compositional gap that separates the rhyolites from the other BSC lavas (Figs. 5 and 6), we consider a cogenetic relationship with the basalts questionable. Melting of an amphibole-bearing lower-crustal source may be a better explanation than extensive crystal fractionation for derivation of the felsic rocks.

We also investigated the possibility that isotopic variation within the basalts is the result of assimilation-fractional crystallization (AFC) of Mesozoic basement rock (DePaolo, 1981). Our AFC modeling, using the most radiogenic Mesozoic arkose (08RR1001; Sisson et al., 2014) over a range of R (mass assimilated/mass crystallized) and f (melt fraction

Downloaded from http://pubs.geoscienceworld.org/gsa/lithosphere/article-pdf/10/6/792/4556618/792.pdf
by guest

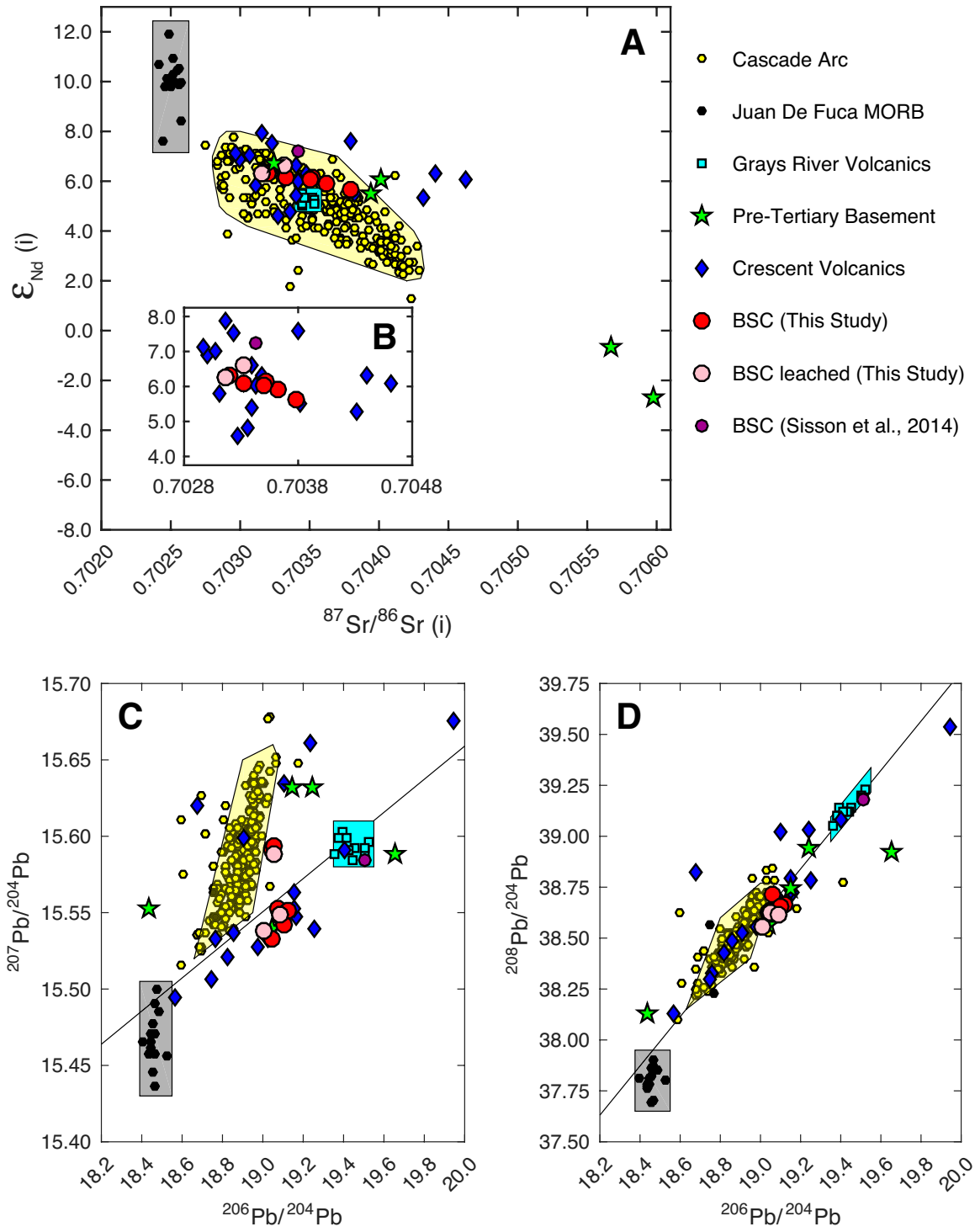

Figure 7. (A) initial $^{87}Sr/^{86}Sr$ vs. initial ε_{Nd} for the Basalt of Summit Creek (BSC) and other rocks from the region. (B) Enlargement focusing on all BSC data to show internal variation. (C) $^{207}Pb/^{204}Pb$ vs. $^{206}Pb/^{204}Pb$. BSC samples that lie above the Northern Hemisphere reference line (NHRL) show evidence for involvement of a subduction component. (D) $^{208}Pb/^{204}Pb$ vs. $^{206}Pb/^{204}Pb$. Note that BSC data are within the range of Crescent Formation basalt data. Regional isotopic data and sources are available in the online regional data supplemental material in the Data Repository (see text footnote 1). Leached BSC samples are similar in composition to the most-depleted Crescent basalts. MORB—mid-ocean-ridge basalt.

Downloaded from http://pubs.geoscienceworld.org/gsa/lithosphere/article-pdf/10/6/792/4556618/792.pdf
by guest

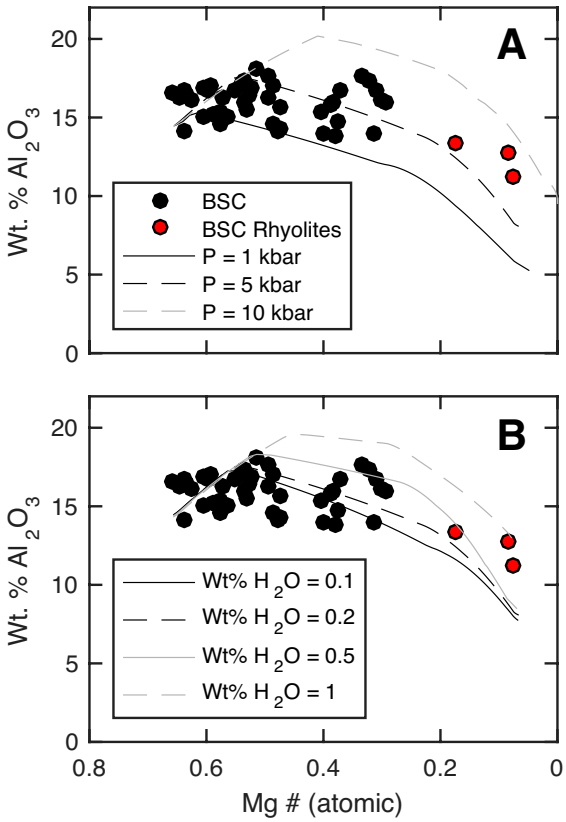

Figure 8. Modeled melt evolution during crystallization for an assumed Basalt of Summit Creek (BSC) parental melt. Melt compositions were calculated using MELTS (Ghiorso and Sack, 1995). (A) Variable pressure, 1.0–10 kbar, at 0.2 wt% H_2O. (B) Variable H_2O content, 0.1–1.0 wt%, at 5 kbar. Most whole-rock compositions for the BSC fall along trends best modeled by melt evolution at 1–5 kbar with a magmatic H_2O content of 0.1–0.5 wt%.

remaining) values, failed to reproduce the observed Sr-Nd isotopic variations except in cases where extreme distribution coefficients ($\bar{D}_{Sr}$ >20) were used. These modeling results and the lack of a correlation between isotopic enrichment and degree of differentiation suggest that assimilation of basement rock was not the primary cause of Sr-Nd isotopic variation among BSC samples. Mantle source heterogeneity (discussed below) and low-temperature alteration that preferentially affected Sr are more likely explanations, the latter of which is consistent with our leaching experiments and with high $\delta^{18}O$ values reported for the BSC and other Eocene rock units in the area (Sisson et al., 2014).

Mantle Sources and Heterogeneity

The majority of BSC samples are modestly LREE enriched and have convex, OIB-like patterns on MORB-normalized spidergrams (Fig. 6). Pb isotope compositions of BSC lavas lie along or slightly below the NHRL, are more radiogenic than Juan de Fuca MORB, are less radiogenic than the plume-influenced Grays River Basalts, and are distinct from the field of Cascade arc rocks (Figs. 7C and 7D). Taken together, these chemical and isotopic data indicate that the majority of BSC lavas were derived from an enriched MORB (E-MORB) source that lacked residual garnet.

For most BSC lavas, the traits described above and the absence of Ta-Nb depletions (Fig. 6B) suggest that the subduction-modified mantle wedge was not a source component. MELTS modeling, which suggests parental magmas had <0.5% H_2O, further indicates that the source was relatively anhydrous. However, a few lavas have elevated $^{207}Pb/^{204}Pb$ and HFSE depletions, which point to involvement of a source with a subduction signature, most likely mantle wedge that was modified during earlier subduction. Alternatively, the Pb isotope compositions of these samples, which are shifted toward the compositions of local Mesozoic sedimentary basement rock (Sisson et al., 2014), could be a result of crustal contamination. However, crustal contamination is less likely given that these samples display minimal evidence of fractionation (e.g., high Cr, Eu/Eu* ~1).

Heterogeneity of the mantle source may also account for some of the incompatible trace-element variations observed among BSC samples. For example, the diversity in Rb and K_2O contents among BSC lavas could reflect variable alkali depletion of the source. An alternative possibility is that K_2O and Rb were removed during alteration. However, alteration is unlikely to produce the corresponding depletions in LREEs and HFSEs, and there is no observed difference in LOI measurements between samples with and without alkali depletion.

Relationship to the Crescent Formation Basalts

A notable feature of BSC lavas is their chemical and isotopic similarity to basalts of the Crescent Formation, which are of the same age but crop out ~100 km to the west. On variation diagrams, the two units show extensive overlap in both major- and trace-element composition (Fig. 5). Samples from both units also have similar LREE enrichments and similar diversity in K and Rb concentrations that can be divided into K- and Rb-depleted and K- and Rb-undepleted groups as described above for the BSC (Figs. 6A and 6B). Sr-Nd-Pb isotopic compositions of BSC samples are within the range of data for Crescent samples but less diverse (Fig. 7). Some of the isotopic diversity seen in Crescent samples, in particular, those samples with $^{87}Sr/^{86}Sr$ >0.704, is probably due to seawater interaction (James et al., 2003). The subaerial BSC samples would not have experienced such alteration and thus have a more limited range of Sr isotopic compositions. Overall, the similarities in age and composition between the BSC and Crescent Formation basalts suggest both units shared a common or at least similar mantle source that was enriched relative to MORB source mantle and moderately heterogeneous in composition.

The age and petrologic similarities of the BSC to Crescent Formation lavas raise the possibility that the BSC could be a displaced block of Crescent Formation that was thrust ~100 km inland. Seven lines of evidence argue against this hypothesis: (1) There is no indication of large-scale faulting or deformation within or at the base of BSC, and the contact with the underlying Mesozoic rocks is mapped as depositional (Schasse, 1987; Vance et al., 1987). (2) Fluvial sediments interbedded with BSC lavas near the base of the section contain clasts derived from the nearby Mesozoic basement (Vance et al., 1987). These sediments are also lithologically distinct from turbidites and other marine sediments associated with the Crescent Formation (Babcock et al., 1994). (3) BSC flows have the same steep westward dips as the overlying Ohanapecosh Formation, suggesting that the deformation that tilted the BSC did not occur until after Ohanapecosh deposition in the Oligocene. (4) BSC lavas differ from those of the Crescent Formation in that they are entirely subaerial and do not preserve Sr isotopic evidence of interaction with seawater. (5) BSC lavas display no evidence of the prehnite-pumpellyite-facies to lower-amphibolite-facies and lower-blueschist-facies metamorphism that affected the Crescent Formation (Timpa et al., 2005; Hirsch and Babcock, 2009). (6) A few BSC samples show elemental and/or isotopic evidence of derivation from subduction-modified mantle and/or contamination by arc crust, which is known to exist beneath the Summit Creek area (Sisson et al., 2014).

Downloaded from http://pubs.geoscienceworld.org/gsa/lithosphere/article-pdf/10/6/792/4556618/792.pdf
by guest

Similar arc signatures are unknown among Crescent lavas. (7) Seismic data (Obrebski et al., 2014) indicate that Siletzia does not extend in the subsurface beneath the Mount Rainier area, which also encompasses the Summit Creek area. In summary, field, geochemical, isotopic, and geophysical data all suggest that while BSC lavas originated from similar mantle sources as the Crescent Formation basalts, they erupted in their present setting well inboard of the continental margin.

Tectonic Setting

The tectonic setting in which BSC lavas erupted is constrained by four main observations: (1) The vast majority of these lavas are chemically and isotopically similar to basalts of the Crescent Formation, most likely reflecting a similar petrogenesis. (2) They were emplaced in the forearc region of an active subduction zone (Ewing, 1980; Madsen et al., 2006). (3) They ascended through the mantle wedge but display no chemical signatures that characterize arc magmas. (4) They predate the oldest Cascade arc rocks by >4 m.y. Taken together, these constraints require a mechanism whereby asthenospheric mantle was able to rise through the subducting slab and undergo partial melting during ascent through the wedge without incorporating metasomatized mantle. During the Eocene, two possible tectonic scenarios could meet these requirements: tearing of the Farallon slab (Sigloch et al., 2008; Schmandt and Humphreys, 2011), and passage of a slab window (Thorkelson and Taylor, 1989; Breitsprecher et al., 2003; Madsen et al., 2006). In both scenarios, a discontinuity in the downgoing slab would allow asthenospheric mantle to rise into the mantle wedge and undergo decompression melting.

Alternatively, lavas with MORB- or OIB-like compositions can originate in arcs through melting of heterogeneous mantle sources (Leeman et al., 1990; Jagoutz et al., 2011). Some Quaternary low-K olivine tholeiites in the southern Washington Cascades are broadly similar in composition, although not identical, to the BSC (Leeman et al., 2005). This raises the possibility that BSC magmas could have originated within the mantle wedge, eliminating the need for a break in the slab. However, this scenario requires that mantle indistinguishable from the Crescent basalt source was present in the wedge prior to the accretion of Siletzia, and it underwent melting immediately afterward. While such a process cannot be unequivocally ruled out, during this period rapid, low-angle subduction would have served to both cool the mantle wedge and reduce its thickness. This would have inhibited melting of the mantle wedge and probably explains the scarcity of magmatism in western Washington between 65 Ma and accretion of the Siletzia terrane (Gutscher et al., 2000; Miller et al., 2016).

Instead, we suggest that BSC magmatism was a consequence of slab breakoff. Slab breakoff occurs when buoyant material, such as continental crust, an island arc, an oceanic plateau, or young lithosphere, approaches the trench and resists subduction. The continued downward force of slab pull leads to necking and then tearing (detachment) of the subducted portion of the plate, which can trigger mantle upwelling and subsequent magmatism (Davies and von Blanckenburg, 1995). In the northwestern United States, this would have occurred when Siletzia was accreted to the continental margin at ca. 50 Ma. Evidence of slab detachment in this case is provided by seismic tomography, which reveals a high-velocity "curtain" extending to ~600 km depth beneath Idaho; this "curtain" is interpreted as a stalled remnant of the Farallon plate that broke off after Siletzia accretion (Sigloch et al., 2008; Schmandt and Humphreys, 2011).

The forearc setting of BSC volcanism and its timing relative to Siletzia accretion are consistent with a breakoff model based on comparisons with: (1) other localities where magmatism is attributed to this process, and (2) the results of numerical modeling in the literature. Miocene forearc volcanism in Baja California, which has been linked to slab breakoff (Pallares et al., 2007), represents a possible analog for the BSC. Normal calc-alkaline volcanism in Baja largely ceased ca. 12.5 Ma as the Pacific-Farallon oceanic spreading ridge approached the subduction zone, and it was followed by forearc magmatism that lacked arc traits from ca. 14.2 to 7.5 Ma. These forearc rocks define a belt ~600 km long and ~100 km wide along which magmatism was roughly synchronous. This belt lies 100–200 km inboard of the trench and developed very shortly after the cessation of normal arc magmatism; it is inferred to overlie the gap that opened where the slab detached. The size, location relative to the trench, timing relative to accretion, and chemical traits of Baja forearc magmatism are similar to those of the BSC and the other Eocene belt units emplaced in Washington, suggesting that these units also formed in a slab breakoff setting.

Results of modeling predict that breakoff should occur from <5 to >20 m.y. after the onset of collision and at depths of 35–300 km. However, there is general agreement that breakoff occurs earlier and at shallower levels for younger, slower, warmer, and/or weaker slabs (van de Zedde and Wortel, 2001; Andrews and Billen, 2009; van Hunen and Allen, 2011; Duretz et al., 2014). For situations involving accretion of a spreading ridge, a scenario that may be analogous to the accretion of Siletzia, three-dimensional models predict that strain within the slab becomes great enough to slow subduction when the ridge is within 150 km of the trench, and that the subducted slab will break off within 2 m.y. of initial slowing, when the ridge is 100–115 km from the trench. Tearing is predicted at a depth of 40–55 km and 190–225 km inboard of the trench (Burkett and Billen, 2010). Both the timing and location of BSC eruptions are consistent with these models.

Magmas generated in response to slab breakoff are compositionally diverse and result in short-lived, linear magmatic belts. Davies and von Blanckenburg (1995) suggested that elevated heat flow commonly results in melting of the metasomatized mantle wedge and overlying crust rather than the upwelling asthenosphere itself, and consequently the magmatism tends to be calc-alkaline and felsic. However, where breakoff occurs at shallow depths, as is predicted for a warm young slab, the upwelling asthenosphere may undergo melting and produce magmas with tholeiitic or alkaline compositions (Davies and von Blanckenburg, 1995; van de Zedde and Wortel, 2001). This has been documented in areas of suspected breakoff magmatism, including Newfoundland (Whalen et al., 1996) and Baja California (Ferrari, 2004; Pallares et al., 2007). Thus, the compositions of BSC magmas are consistent with those observed in other areas with suspected breakoff-induced magmatism, and specifically those where breakoff is thought to have occurred at shallow depth.

An alternative tectonic scenario for BSC magmatism is passage of a slab window, an event that has been proposed as the cause of widespread Eocene extension and magmatism in Washington and British Columbia (Haeussler et al., 2003; Madsen et al., 2006). Eruption of basalts with oceanic affinities in the forearc has been attributed to slab window magmatism in a number of arcs, including the Cascades (Chan et al., 2012). Plate-motion reconstructions indicate that the Kula-Farallon and/or Kula-Resurrection Ridges intersected with the North American margin near the latitude of Washington, Oregon, and British Columbia during the Eocene, producing one or more slab windows (Babcock et al., 1992; Breitsbacher et al., 2003; Haeussler et al., 2003; Madsen et al., 2006). However, their precise locations and orientations through time are not well constrained.

Although the location and petrologic characteristics of the BSC are compatible with either a slab window or slab breakoff model, four lines of evidence favor the latter: (1) After Siletzia was accreted, the Cascadia subduction zone jumped westward to its present position. This shift must have been preceded by slab breakoff and was coincident in time with the eruption of the BSC. (2) Between ca. 53 and 45 Ma, a wave of dynamic/

Downloaded from http://pubs.geoscienceworld.org/gsa/lithosphere/article-pdf/10/6/792/4556618/792.pdf
by guest

thermal uplift (Smith et al., 2014) and magmatism (Tepper, 2016) migrated southwestward (trenchward) across the northwestern United States. This activity is attributed to rollback of the Farallon slab following the accretion of Siletzia, and in other arcs, rollback has been identified as a precursor to slab breakoff (Lucente and Margheriti, 2008; Ozawa et al., 2015). (3) Trenchward migration of uplift and magmatism was roughly perpendicular to the margin, which one would not expect from a migrating slab window, because a slab window would have a significant component of margin-parallel motion. (4) Seismic images of detached Farallon slab fragments (Sigloch et al., 2008; Schmandt and Humphreys, 2011) provide independent evidence of slab breakoff.

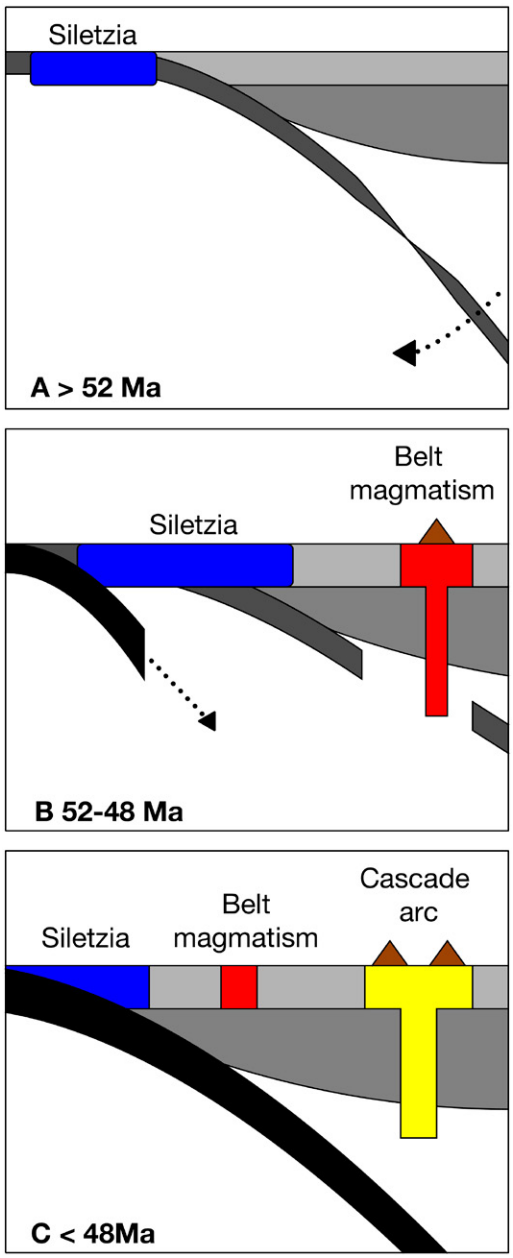

Figure 9. Tectonic setting and origin of the Basalt of Summit Creek (BSC). (A) Prior to 52 Ma: Near-trench magmatism is absent due to flat subduction of the Farallon slab. As Siletzia approaches, the trench subduction slows, while already subducted crust continues sinking into the mantle. Resulting tension leads to rollback, thinning, and eventual tearing of the slab. (B) 52–48 Ma: Mantle upwelling through the torn slab results in a short-lived linear belt of magmatism, which includes the BSC. During this time, subduction is initiated outboard of Siletzia. (C) Subsequent to 48 Ma: Resumed subduction results in the earliest Cascade arc magmatism ca. 44 Ma.

SUMMARY AND CONCLUSIONS

A growing body of geochemical, geophysical, and geochronological data, combined with new reconstructions of plate motions, provides support for the hypothesis that the Coast Range basalts of Oregon and Washington originated as an oceanic plateau or chain of islands that was accreted to the margin of North America (e.g., Wells et al., 2014). The accretion of this oceanic terrane, Siletzia, was a significant episode in the Tertiary geologic history of the northwestern United States and British Columbia, but the details of the event, and of its broader impact throughout the region, are only now beginning to emerge (Johnston and Acton, 2003; Wells et al., 2014; Eddy et al., 2016; Tepper, 2016).

Breakoff of the subducting Farallon slab would have been one of the consequences of Siletzia accretion (Fig. 9A), and high-velocity seismic domains in the mantle beneath eastern Washington and Idaho have been interpreted as remnants of this slab (Sigloch et al., 2008; Schmandt and Humphreys, 2011). Another geological manifestation of slab breakoff is a short-lived linear belt of igneous activity localized above the region where asthenospheric mantle upwells through the zone of rupture. We suggest that the BSC is part of such a belt, not previously recognized, that roughly follows the leading subsurface edge of Siletzia for >150 km in western Washington (Figs. 1 and 9B). Evidence supporting a slab breakoff origin for the BSC and other units within this belt includes their restricted range of ages (50–48 Ma; coincident with or slightly after Siletzia accretion), which appear synchronous along its length, their location (in the former forearc region), and their petrologic traits (some units with MORB-OIB affinities, others with crustal melting signatures). Eventually, subduction resumed outboard of the accreted terrane, resulting in renewed arc magmatism. In Washington, this resulted in the earliest Cascade arc magmatism at ca. 44 Ma (Fig. 9C; Christiansen and Yeats, 1992; Sherrod and Smith, 2000; MacDonald et al., 2013; Dragovich et al., 2016).

The BSC represents an important link between magmatic and tectonic events occurring along the continental margin and those occurring further inboard. Age constraints provided by these lavas combined with improved knowledge of the timing of Siletzia accretion (Wells et al., 2014; Eddy et al., 2016) make it possible to better assess the extent to which slab breakoff, likely accompanied by rollback, might have been responsible for other geologic events, in particular, magmatism, extension, and uplift, that occurred in Washington, Oregon, and British Columbia during the Eocene.

ACKNOWLEDGMENTS

Funding for this research was provided by National Science Foundation (NSF) grants EAR-1119252 to J. Tepper and EAR-1118883 to S. Bowring. We thank Ken Clark, Mike Valentine, and Sam Berkelhammer for assistance in the field. Eddy is indebted to S. Bowring for support and encouragement during the early parts of this project. We also acknowledge the Fall 2010 Igneous Petrology class at the University of Puget Sound (Tacoma, Washington) for the data they collected; this study began as their class project. We also thank K. Stuewe, E. Todd, D. Canil, and an anonymous reviewer for their thoughtful comments.

REFERENCES CITED

Andrews, E.R., and Billen, M.I., 2009, Rheologic controls on the dynamics of slab detachment: Tectonophysics, v. 464, p. 60–69, https://doi.org/10.1016/j.tecto.2007.09.004.

Babcock, R.S., Burmester, R.F., Engebretson, D.C., and Warnock, A., 1992, A rifted margin origin for the Crescent Basalts and related rocks in the Northern Coast Range Volcanic Province, Washington and British Colombia: Journal of Geophysical Research, v. 97, p. 6799–6821, https://doi.org/10.1029/91JB02926.

Downloaded from http://pubs.geoscienceworld.org/gsa/lithosphere/article-pdf/10/6/792/4556618/792.pdf
by guest

Babcock, R.S., Suczek, C.A., and Engebretson, D.C., 1994, The Crescent "Terrane," Olympic Peninsula and Southern Vancouver Island: Washington Division of Geology and Earth Resources Bulletin 80, p. 141–157.

Bordet, E., Mihalynuk, M.G., Hart, C.J.R., Mortensen, J.K., Friedman, R.M., and Gabites, J., 2014, Chronostratigraphy of Eocene volcanism, central British Columbia: Canadian Journal of Earth Sciences (Revue Candienne des Sciences de la Terre), v. 51, p. 56–103, https://doi.org/10.1139/cjes-2013-0073.

Bowring, J.F., McLean, N.M., and Bowring, S.A., 2011, Engineering cyber infrastructure for U-Pb geochronology: Tripoli and U-Pb_Redux: Geochemistry Geophysics Geosystems, v. 12, Q0AA19, https://doi.org/10.1029/2010GC003479.

Brach-Papa, C., Van Bocxstaele, M., Ponzevera, E., and Quétel, C.R., 2009, Fit for purpose validated method for the determination of the strontium isotopic signature in mineral water samples by multi-collector–inductively coupled plasma–mass spectrometry: Spectrochimica Acta B–Atomic Spectroscopy, v. 64, p. 229–234, https://doi.org/10.1016/j.sab.2009.01.012.

Breitsprecher, K., Thorkelson, D.J., Groome, W.G., and Dostal, CJ., 2003, Geochemical confirmation of the Kula-Farallon slab window beneath the Pacific Northwest in Eocene time: Geology, v. 31, p. 351–354, https://doi.org/10.1130/0091-7613(2003)031<0351:GCOTKF>2.0.CO;2.

Burkett, E.R., and Billen, M.I., 2010, Three-dimensionalitiy of slab detachment due to ridge-trench collision: Laterally simultaneous boudinage versus tear propagation: Geochemistry Geophysics Geosystems, v. 11, Q11012, https://doi.org/10.1029/2010GC003286.

Chan, C.F., Tepper, J.H., and Nelson, B.K., 2012, Petrology of the Grays River volcanics, southwest Washington: Plume-influenced slab window magmatism in the Cascadia forearc: Geological Society of America Bulletin, v. 124, p. 1324–1338, https://doi.org/10.1130/B30576.1.

Christiansen, R.L., and Yeats, R.S., 1992, Post-Laramide geology of the U.S. Cordillera region, *in* Burchfiel, B.C., Lipman, P.W., and Zoback, M.L., eds., The Cordilleran Orogen: Conterminous U.S.: Boulder, Colorado, Geological Society of America, The Geology of North America, v. G-3, p. 261–406.

Condon, D.J., Schoene, B., McLean, N.M., Bowring, S.A., and Parrish, R.R., 2015, Metrology and traceability of U-Pb isotope dilution geochronology (EARTHTIME tracer calibration Part I): Geochimica et Cosmochimica Acta, v. 164, p. 464–480, https://doi.org/10.1016/j.gca.2015.05.026.

Davidson, J., Turner, S., Handley, H., Macpherson, C., and Dosseto, A., 2007, Amphibole "sponge" in arc crust?: Geology, v. 35, p. 787–790, https://doi.org/10.1130/G23637A.1.

Davies, J.H., and von Blanckenburg, F., 1995, Slab breakoff: A model of lithosphere detachment and its test in the magmatism and deformation of collisional orogens: Earth and Planetary Science Letters, v. 129, p. 85–102, https://doi.org/10.1016/0012-821X(94)00237-S.

DePaolo, D.J., 1981, Trace element and isotopic effects of combined wall rock assimilation and fractional crystallization: Earth and Planetary Science Letters, v. 53, p. 189–202, https://doi.org/10.1016/0012-821X(81)90153-9.

Dickinson, W.R., and Snyder, W.S., 1978, Plate tectonics of the Laramide orogeny *in* Matthews, V., III, ed., Laramide Folding Associated with Basement Block Faulting in the Western United States: Geological Society of America Memoir 151, p. 355–366.

Doe, B.R., 1994, Zinc, copper, and lead in mid-ocean ridge basalts and the source rock control on Zn/Pb in ocean-ridge hydrothermal deposits: Geochimica et Cosmochimica Acta, v. 58, p. 2215–2223, https://doi.org/10.1016/0016-7037(94)90006-X.

Dostal, J., Robichaud, D.A., Church, B.N., and Reynolds, P.H., 1998, Eocene Challis-Kamloops volcanism in central British Columbia: An example from the Buck Creek basin: Canadian Journal of Earth Sciences (Revue Candienne des Sciences de la Terre), v. 35, p. 951–963, https://doi.org/10.1016/0012-821X(81)90153-9.

Dragovich, J.D., Mavor, S.P., Anderson, M.L., Mahan, S.A., MacDonald, J.H., Jr., Tepper, J.H., Smith, D.T., Stoker, B.A., Koger, C.J., Cakir, R., DuFrane, S.A., Scott, S.P., and Justman, B.J., 2016, Geologic Map of the Granite Falls 7.5-Minute Quadrangle, Snohomish County, Washington: Washington Division of Geology and Earth Resources Map Series 2016–03, scale 1:24,000, 1 sheet, 63 p. text.

Dumitru, T.A., Ernst, W.G., Wright, J.E., Wooden, J.L., Wells, R.E., Farmer, L.P., Kent, A.J.R., and Graham, S.A., 2013, Eocene extension in Idaho generated massive sediment floods into the Franciscan Trench and into the Tyee, Great Valley, and Green River Basins: Geology, v. 41, p. 187–190, https://doi.org/10.1130/G33746.1.

Duncan, R.A., 1982, A captured island chain in the Coast Range of Oregon and Washington: Journal of Geophysical Research–Solid Earth, v. 87, p. 10,827–10,837, https://doi.org/10.1029/JB087iB13p10827.

Duretz, T., Gerya, T.V., and Spakman, W., 2014, Slab detachment in laterally varying subduction zones: 3-D numerical modeling: Geophysical Research Letters, v. 41, p. 1951–1956, https://doi.org/10.1002/2014GL059472.

Eddy, M.P., Bowring, S.A., Umhoefer, P.J., Miller, R.B., McLean, N.M., and Donaghy, E.E., 2016, High-resolution temporal and stratigraphic record of Siletzia's accretion and triple junction migration from nonmarine sedimentary basins in central and western Washington: Geological Society of America Bulletin, v. 128, p. 425–441, https://doi.org/10.1130/B31335.1.

Eddy, M.P., Clark, K.P., and Polenz, M., 2017, Age and volcanic stratigraphy of the Eocene Siletzia oceanic plateau in Washington and on Vancouver Island: Lithosphere, v. 9, p. 652–664, https://doi.org/10.1130/L650.1.

Evans, J.E. and Ristow R.J. Jr., 1994, Depositional history of the southeastern outcrop belt of the Chuckanut Formation: Implications for the Darrington–Devil's Mountain and Straight Creek fault zones, Washington (U.S.A.): Canadian Journal of Earth Sciences (Revue Candienne des Sciences de la Terre), v. 31, p. 1727–1743, https://doi.org/10.1139/e94-154.

Ewing, T.E., 1980, Paleogene tectonic evolution of the Pacific Northwest: The Journal of Geology, v. 88, p. 619–638, https://doi.org/10.1086/628551.

Ferrari, L., 2004, Slab detachment control on mafic volcanic pulse and mantle heterogeneity in central Mexico: Geology, v. 32, p. 77–80, https://doi.org/10.1130/G19887.1.

Gaffney, A.M., Blichert-Toft, J., Nelson, B.K., Bizzarro, M., Rosing, M., and Albarède, F., 2007, Constraints on source-forming processes of West Greenland kimberlites inferred from Hf-Nd isotope systematics: Geochimica et Cosmochimica Acta, v. 71, p. 2820–2836, https://doi.org/10.1016/j.gca.2007.03.009.

Ghiorso, M.S., and Sack, R.O., 1995, Chemical mass transfer in magmatic processes. IV. A revised and internally consistent thermodynamic model for the interpolation and extrapolation of liquid-solid equilibria in magmatic systems at elevated temperatures and pressures: Contributions to Mineralogy and Petrology, v. 119, p. 197–212, https://doi.org/10.1007/BF00307281.

Gordon, S.M., Grove, M., Whitney, D.L., Schmitt, A.K., and Teyssier, C., 2009, Fluid-rock interaction in orogenic crust tracked by zircon depth profiling: Geology, v. 37, p. 735–738, https://doi.org/10.1130/G25597A.1.

Gutscher, M.-A., Maury, R., Eissen, J.-P., and Bourdon, E., 2000, Can slab melting be caused by flat subduction?: Geology, v. 28, p. 535–538, https://doi.org/10.1130/0091-7613(2000)28<535:CSMBCB>2.0.CO;2.

Haeussler, P.J., Bradley, D.C., Wells, R.E., and Miller, M.L., 2003, Life and death of the Resurrection plate: Evidence for its existence and subduction in the northeastern Pacific in Paleocene–Eocene time: Geological Society of America Bulletin, v. 115, p. 867–880, https://doi.org/10.1130/0016-7606(2003)115<0867:LADOTR>2.0.CO;2.

Haileab, B., Denny, A., and Harrison, B.K., 2012, Expanded geochemical analysis of the Eocene Crescent Formation, Olympic Peninsula, Washington: San Francisco, California, American Geophysical Union, 2012 Fall Meeting supplement, abstract V13B–2853.

Harkins, S.A., Appold, M.S., Nelson, B.K., Brewer, A.M., and Groves, I.M., 2008, Lead isotope constraints on the origin of nonsulfide zinc and sulfide zinc-lead deposits in the Flinders Ranges, South Australia: Economic Geology and the Bulletin of the Society of Economic Geologists, v. 103, p. 353–364, https://doi.org/10.2113/gsecongeo.103.2.353.

Hart, S.R., 1984, A large-scale isotope anomaly in the Southern Hemisphere mantle: Nature, v. 309, p. 753–757, https://doi.org/10.1038/309753a0.

Hegner, E., and Tatsumoto, M., 1987, Pb, Sr, Nd isotopes in basalts and sulfides from the Juan de Fuca Ridge: Journal of Geophysical Research, v. 92, p. 11,380–11,386, https://doi.org/10.1029/JB092iB11p11380.

Hiess, J., Condon, D.J., McLean, N., and Noble, S.R., 2012, $^{238}U/^{235}U$ systematics in terrestrial uranium-bearing minerals: Science, v. 335, p. 1610–1614, https://doi.org/10.1126/science.1215507.

Hirsch, D.M., and Babcock, R.S., 2009, Spatially heterogenenous burial and high *P/T* metamorphism in the Crescent Formation, Olympic Peninsula, Washington: The American Mineralogist, v. 94, p. 1103–1110, https://doi.org/10.2138/am.2009.3187.

Irvine T.N., and Baragar, W.R.A., 1971, A guide to the chemical classification of common volcanic rocks: Canadian Journal of Earth Sciences (Revue Candienne des Sciences de la Terre), v. 8, p. 523–548, https://doi.org/10.1139/e71-055.

Jaffey, A.H., Flynn, K.F., Glendenin, L.E., Bentley, W.C., and Essling, A.M., 1971, Precision measurement of half-lives and specific activities of ^{235}U and ^{238}U: Physical Review C: Nuclear Physics, v. 4, p. 1889–1906, https://doi.org/10.1103/PhysRevC.4.1889.

Jagoutz, O., Müntener, O., Schmidt, M.W., and Burg, J.-P., 2011, The roles of flux- and decompression melting and their respective fractionation lines for continental crust formation: Evidence from the Kohistan arc: Earth and Planetary Science Letters, v. 303, p. 25–36, https://doi.org/10.1016/j.epsl.2010.12.017.

James, R.H., Allen, D.E., and Seyfried, W.E., 2003, An experimental study of alteration of oceanic crust and terrigenous sediments at moderate temperatures (51 to 350°C): Insights as to chemical processes in near-shore ridge-flank hydrothermal systems: Geochimica et Cosmochimica Acta, v. 67, p. 681–691, https://doi.org/10.1016/S0016-7037(02)01113-4.

Johnston, S.T., and Acton, S., 2003, The Eocene southern Vancouver island orocline—A response to seamount accretion and the cause of fold-and-thrust belt and extensional basin formation: Tectonophysics, v. 365, p. 165–183, https://doi.org/10.1016/S0040-1951(03)00021-0.

Kruckenberg, S.C., Whitney, D.L., Teyssier, C., Fanning, F., and Dunlap, W.J., 2008, Paleocene–Eocene migmatite crystallization, extension and exhumation in the hinterland of the northern Cordillera: Okanogan dome, Washington, USA: Geological Society of America Bulletin, v. 120, p. 912–929, https://doi.org/10.1130/B26153.1.

LeBas, M.J., LeMaitre, R.W., Streckeisen, A., and Zanettin, B., 1986, A chemical classification of volcanic rocks based on the total alkali-silica diagram: Journal of Petrology, v. 27, p. 745–750, https://doi.org/10.1093/petrology/27.3.745.

Leeman, W.P., Smith, D.R., Hildreth, W., Palacz, Z., and Rogers, N., 1990, Compositional diversity of late Cenozoic basalts in a transect across the southern Washington Cascades: Implications for subduction zone magmatism: Journal of Geophysical Research, v. 95, p. 19,561–19,582, https://doi.org/10.1029/JB095iB12p19561.

Leeman, W.P., Lewis, J.F., Evarts, R.C., Conrey, R.M., and Streck, M.J., 2005, Petrologic constraints on the thermal structure of the Cascade arc: Journal of Volcanology and Geothermal Research, v. 140, p. 67–105, https://doi.org/10.1016/j.jvolgeores.2004.07.016.

Lucente, F.P., and Margheriti, L., 2008, Subduction rollback, slab breakoff, and induced strain in the uppermost mantle beneath Italy: Geology, v. 36, p. 375–378, https://doi.org/10.1130/G24529A.1.

MacDonald, J.H., Dragovich, J.D., Littke, H.A., Anderson, M., and Dufrane, S.A., 2013, The Eocene volcanic rocks of Mount Persis: An Eocene continental arc that contains adakitic magmas: Geological Society of America Abstracts with Programs, v. 45, no. 7, p. 392.

Machlus, M.L., Ramezani, J., Bowring, S.A., Hemming, S.R., Tsukui, K., and Clyde, W.C., 2015, A strategy for cross-calibrating U-Pb chronology and astrochronology of sedimentary sequences: An example from the Green River Formation, Wyoming, USA: Earth and Planetary Sciences, v. 413, p. 70–78, https://doi.org/10.1016/j.epsl.2014.12.009.

Madsen, J.K., Thorkelson, D.J., Friedman, R.M., and Marshall, D.D., 2006, Cenozoic to recent plate configurations in the Pacific Basin: Ridge subduction and slab window magmatism in western North America: Geosphere, v. 2, p. 11–34, https://doi.org/10.1130/GES00020.1.

Massey, N.W.D., 1986, Metchosin igneous complex, southern Vancouver Island: Ophiolite stratigraphy developed in an emergent island setting: Geology, v. 14, p. 602–605, https://doi.org/10.1130/0091-7613(1986)14<602:MICSVI>2.0.CO;2.

Downloaded from http://pubs.geoscienceworld.org/gsa/lithosphere/article-pdf/10/6/792/4556618/792.pdf
by guest

Mattinson, J.M., 2005, Zircon U-Pb chemical abrasion ("CA-TIMS") method: Combined annealing and multi-step partial dissolution analysis for improved precision and accuracy of zircon ages: Chemical Geology, v. 220, p. 47–66, https://doi.org/10.1016/j.chemgeo.2005.03.011.

McCrory, P.A., and Wilson, D.S., 2013, A kinematic model for the formation of the Siletz-Crescent forearc terrane by capture of coherent fragments of the Farallon and Resurrection plates: Tectonics, v. 32, p. 718–736, https://doi.org/10.1002/tect.20045.

McDonough, W.F., and Sun, S.-s., 1995, Composition of the Earth: Chemical Geology, v. 120, p. 223–253, https://doi.org/10.1016/0009-2541(94)00140-4.

McLean, N.M., Bowring, J.F., and Bowring, S.A., 2011, An algorithm for U-Pb isotope dilution data reduction and uncertainty propagation: Geochemistry Geophysics Geosystems, v. 12, Q0AA18, https://doi.org/10.1029/2010GC003478.

McLean, N.M., Condon, D.J., Schoene, B., and Bowring, S.A., 2015, Evaluating uncertainties in the calibration of isotopic reference materials and multi-element isotopic tracers (EARTHTIME tracer calibration part II): Geochimica et Cosmochimica Acta, v. 164, p. 481–501, https://doi.org/10.1016/j.gca.2015.02.040.

Miller, R.B., 1989, The Mesozoic Rimrock Lake inlier, southern Washington Cascades: Implications for the basement to the Columbia Embayment: Geological Society of America Bulletin, v. 101, p. 1289–1305, https://doi.org/10.1130/0016-7606(1989)101<1289:TMRLIS>2.3.CO;2.

Miller, R.B., Gordon, S.M., Bowring, S., Doran, B., McLean, N., Michels, Z., Shea, E., and Whitney, D.L., 2016, Linking deep and shallow crustal processes during regional transtension in an exhumed continental arc, North Cascades, northwestern Cordillera (USA): Geosphere, v. 12, p. 900–924, https://doi.org/10.1130/GES01262.1.

Moothart, S.R., 1993, Geology of the Middle and Upper Eocene Mcintosh Formation and Adjacent Volcanic and Sedimentary Rock Units, Willapa Hills, Pacific County, Southwest Washington [M.S. thesis]: Corvallis, Oregon, Oregon State University, 265 p.

Morris, G.A., Larson, P.B., and Hooper, P.R., 2000, 'Subduction style' magmatism in a non-subduction setting: The Colville igneous complex, NE Washington State, USA: Journal of Petrology, v. 41, p. 43–67, https://doi.org/10.1093/petrology/41.1.43.

Muller, J.E., 1980, Chemistry and origin of the Eocene Metchosin volcanics, Vancouver Island, British Columbia: Canadian Journal of Earth Sciences, v. 17, p. 199–209, https://doi.org/10.1139/e80-016.

Murphy, J.B., Hynes, A.J., Johnston, S.T., and Keppie, J.D., 2003, Reconstructing the ancestral Yellowstone plume from accreted seamounts and its relationship to flat-slab subduction: Tectonophysics, v. 365, p. 185–194, https://doi.org/10.1016/S0040-1951(03)00022-2.

Nelson, B.K., 1995, Fluid flow in subduction zones: Evidence from neodymium and strontium isotope variations in metabasalts of the Franciscan Complex, California: Contributions to Mineralogy and Petrology, v. 119, p. 247–262, https://doi.org/10.1007/BF00307285.

Obrebski, M., Abers, G.A., and Foster, A., 2014, Magmatic arc structure around Mount Rainier, WA, from the joint inversion of receiver functions and surface wave dispersion: Geochemistry Geophysics Geosystems, v. 16, p. 178–194, https://doi.org/10.1002/2014GC005581.

Ozawa, K., Maekawa, H., Shibata, K., Asahara, Y., and Yoshikawa, M., 2015, Evolution processes of Ordovician-Devonian arc system in the South Kitakami Massif and its relevance to the Ordovician ophiolite pulse: The Island Arc, v. 24, p. 73–118, https://doi.org/10.1111/iar.12100.

Pallares, C., Maury, R.C., Bellon, H., Royer, J.V., Calmus, T., Aguillón-Robles, A., Cotton, J., Benoit, M., Michaud, F., and Bourgois, J., 2007, Slab-tearing following ridge-trench collision: Evidence from Miocene volcanism in Baja California, México: Journal of Volcanology and Geothermal Research, v. 161, p. 95–117, https://doi.org/10.1016/j.jvolgeores.2006.11.002.

Parker, D.F., Hodges, F.N., Perry, A., Mitchener, M.E., Barnes, M.A., and Ren, M., 2010, Geochemistry and petrology of late Eocene Cascade Head and Yachats Basalts and alkali intrusions of the central Oregon Coast Range, U.S.A.: Journal of Volcanology and Geothermal Research, v. 198, p. 311–324, https://doi.org/10.1016/j.jvolgeores.2010.09.016.

Phillips, B.A., Kerr, A.C., Mullen, E.K., and Weis, D., 2017, Oceanic mafic magmatism in the Siletz terrane, NW North America: Fragments of an Eocene oceanic plateau?: Lithos, v. 274–275, p. 291–303, https://doi.org/10.1016/j.lithos.2017.01.005.

Phillips, W.M., Walsh, T.J., and Hagan, R.A., 1988, Eocene Transition from Oceanic to Arc Volcanism, Southwest Washington: U.S. Geological Survey Open-File Report 89-178, p. 199–256.

Pyle, D.G., Duncan, R., Wells, R.E., Graham, D.W., Harrison, B., and Hanan, B., 2009, Siletzia: An oceanic large igneous province in the Pacific Northwest: Geological Society of America Abstracts with Programs, v. 41, no. 7, p. 369.

Schasse, H.W., compiler, 1987, Geologic Map of the Mount Rainier Quadrangle, Washington: Washington Division of Geology and Earth Resources Open-File Report 87-16, 1 plate, scale 1:100,000, 43 p. text.

Schmandt, B., and Humphreys, E., 2011, Seismically imaged relict slab from the 55 Ma Siletzia accretion to the northwest United States: Geology, v. 39, p. 175–178, https://doi.org/10.1130/G31558.1.

Sherrod, D.R., and Smith, J.G., 2000, Geologic Map of Upper Eocene to Holocene Volcanic and Related Rocks of the Cascade Range, Oregon: U.S. Geological Survey Miscellaneous Investigations Series Map I-2569, scale 1:500,000, 1 sheet, 17 p text.

Sigloch, K., McQuarrie, N., and Nolet, G., 2008, Two-stage subduction history under North America inferred from multiple-frequency tomography: Nature Geoscience, v. 1, p. 458–462, https://doi.org/10.1038/ngeo231.

Sisson, T.W., Salters, V.J.B., and Larson, P.B., 2014, Petrogenesis of Mount Rainier andesite: Magma flux and geologic controls on the contrasting differentiation styles at stratovolcanoes of the southern Washington Cascades: Geological Society of America Bulletin, v. 126, p. 122–144, https://doi.org/10.1130/B30852.1.

Smith, M.E., Caroll, A.R., Jicha, B.R., Cassels, E.J., and Scott, J.J., 2014, Paleogeographic record of Eocene Farallon slab rollback beneath western North America: Geology, v. 42, no. 12, p. 1039–1042, https://doi.org/10.1130/G36025.1.

Snavely, P.D., MacLeod, N.S., and Wagner, H.C., 1968, Tholeiitic and alkali basalts of the Eocene Siletz River volcanics, Oregon Coast Range: American Journal of Science, v. 266, p. 454–481, https://doi.org/10.2475/ajs.266.6.454.

Sun, S.-s., and McDonough, W.F., 1989, Chemical and isotopic systematics of oceanic basalts: Implications for mantle composition and processes, *in* Saunders, A.D., and Norry, M.J., eds., Magmatism in the Ocean Basins: Geological Society of London Special Publication 42, p. 313–345, https://doi.org/10.1144/GSL.SP.1989.042.01.19.

Tabor, R.W., Frizzell, V.A., Vance, J.A., and Naeser, C.W., 1984, Ages and stratigraphy of Lower and Middle Tertiary sedimentary and volcanic rocks of the central Cascades, Washington: Application to the tectonic history of the Straight Creek fault: Geological Society of America Bulletin, v. 95, p. 26–44, https://doi.org/10.1130/0016-7606(1984)95<26:AASOLA>2.0.CO;2.

Tabor, R.W., Frizzell, V.A., Booth, D.B., and Waitt, R.B., 2000, Geologic Map of the Snoqualmie Pass 30- by 60-Minute Quadrangle, Washington: U.S. Geological Survey Geologic Investigations Series Map I-2538, scale 1:100,000, 1 sheet, 57 p. text.

Tabor, R.W., Booth, D.B., Vance, J.A., and Ford, A.B., 2002, Geologic Map of the Sauk River 30- by 60-Minute Quadrangle, Washington: U.S. Geological Survey Geologic Investigations Series Map I-2592, scale 1:100,000, 1 sheet, 67 p. text.

Tanner, S.L., and Tepper, J.H., 2016, Between the Crescent and the arc: Petrology of early-to-middle Eocene igneous units in western Washington: Geological Society of America Abstracts with Programs, v. 48, no. 4, paper 25-10, https://doi.org/10.1130/abs/2016CD-274492.

Tepper, J.H., 2016, Eocene breakoff and rollback of the Farallon slab—An explanation for the "Challis event"?: Geological Society of America Abstracts with Programs 48, no. 4, paper 7-1, https://doi.org/10:1130/abs/2016CD-274512.

Tepper, J.H., Nelson, B.K., Clark, K., and Barnes, R.P., 2008, Heterogeneity in mantle sources for Eocene basalts in Washington: Trace element and Sr-Nd isotopic evidence for the Crescent and Teanaway Basalts: San Francisco, California, American Geophysical Union, Fall Meeting supplement, abstract V41D–2121.

Thorkelson, D.J., and Taylor, R.P., 1989, Cordilleran slab windows: Geology, v. 17, p. 833–836, https://doi.org/10.1130/0091-7613(1989)017<0833:CSW>2.3.CO;2.

Timpa, S., Gillis, K.M., and Canil, D., 2005, Accretion-related metamorphism of the Metchosin igneous complex, southern Vancouver Island, British Columbia: Canadian Journal of Earth Sciences (Revue Canadienne des Sciences de la Terre), v. 42, p. 1467–1479, https://doi.org/10.1139/E05-043.

Trehu, A.M., Asudeh, I., Brocher, T.M., Luetgert, J.H., Mooney, W.D., Nabelek, J.L., and Nakamura, Y., 1994, Crustal architecture of the Cascadia forearc: Science, v. 266, p. 237–243, https://doi.org/10.1126/science.266.5183.237.

Vance, J.A., Clayton, G.A., Mattinson, J.M., and Naeser, C.W., 1987, Early and Middle Cenozoic Stratigraphy of the Mount Rainier–Tieton River Area: Southern Washington Cascades: Washington Division of Geology and Earth Resources Bulletin 77, p. 269–290.

van de Zedde, D.M.A., and Wortel, M.J.R., 2001, Shallow slab detachment as a transient source of heat at midlithospheric depths: Tectonics, v. 20, p. 868–882, https://doi.org/10.1029/2001TC900018.

van Hunen, J., and Allen, M.B., 2011, Continental collision and slab break-off: A comparison of 3-D numerical models with observations: Earth and Planetary Science Letters, v. 302, p. 27–37, https://doi.org/10.1016/j.epsl.2010.11.035.

Walsh, T.J., Korosec, M.A., Phillips, W.M., Logan, R.L., and Schasse, H.W., 1987, Geologic Map of Washington Southwest Quadrant: Washington Division of Geology and Earth Resources Geologic Map GM-34, scale 1:250,000, 2 sheets, 28 p. text.

Wells, R., Bukry, D., Friedman, R., Pyle, D., Duncan, R., Haeussler, P., and Wooden, J., 2014, Geologic history of Siletzia, a large igneous province in the Oregon and Washington Coast Range: Correlation to the geomagnetic polarity time scale and implications for a long-lived Yellowstone hotspot: Geosphere, v. 10, p. 692–719, https://doi.org/10.1130/GES01018.1.

Wells, R.E., Engebretson, D.C., Snavely, P.D., and Coe, R.S., 1984, Cenozoic plate motions and the volcano-tectonic evolution of western Oregon and Washington: Tectonics, v. 3, p. 275–294, https://doi.org/10.1029/TC003i002p00275.

Wendt, I., and Carl, C., 1991, The statistical distribution of the mean squared weighted deviation: Chemical Geology, v. 86, p. 275–285, https://doi.org/10.1016/0168-9622(91)90010-T.

Whalen, J.B., Jenner, G.A., Longstaffe, F.J., Robert, F., and Gariepy, C., 1996, Geochemical and isotopic (O, Nd, and Sr) constraints on A-type granite petrogenesis based on the Topsails igneous suite, Newfoundland, Appalachians: Journal of Petrology, v. 37, p. 1463–1489, https://doi.org/10.1093/petrology/37.6.1463.

White, W.M., Hofmann, A.W., and Puchelt, H., 1987, Isotope geochemistry of Pacific mid-ocean ridge basalt: Journal of Geophysical Research, v. 92, p. 4881–4893, https://doi.org/10.1029/JB092iB06p04881.

MANUSCRIPT RECEIVED 17 JANUARY 2018
REVISED MANUSCRIPT RECEIVED 8 AUGUST 2018
MANUSCRIPT ACCEPTED 7 SEPTEMBER 2018

Downloaded from http://pubs.geoscienceworld.org/gsa/lithosphere/article-pdf/10/6/792/4556618/792.pdf
by guest